41 Pages

[redacted]

Copy
RM E53L14b

332

NACA RM E53L14b

NACA



# RESEARCH MEMORANDUM

## EXPERIMENTAL INVESTIGATION AT MACH NUMBERS 1.88, 3.16, AND 3.83 OF PRESSURE DRAG OF WEDGE DIVERTERS SIMULATING BOUNDARY-LAYER-REMOVAL SYSTEMS FOR SIDE INLETS

By Thomas G. Piercy and Harry W. Johnson

Lewis Flight Propulsion Laboratory
Cleveland, Ohio



[redacted]

NATIONAL ADVISORY COMMITTEE
FOR AERONAUTICS

WASHINGTON
February 15, 1954

[redacted]

NATIONAL ADVISORY COMMITTEE FOR AERONAUTICS

RESEARCH MEMORANUDM

# EXPERIMENTAL INVESTIGATION AT MACH NUMBERS 1.88, 3.16, AND 3.83 OF PRESSURE DRAG OF WEDGE DIVERTERS SIMULATING BOUNDARY-LAYER-REMOVAL SYSTEMS FOR SIDE INLETS

By Thomas G. Piercy and Harry W. Johnson

## SUMMARY

An experimental investigation was performed at Mach numbers of 1.88, 3.16, and 3.83 to determine the pressure drag of various wedge diverter configurations applicable to boundary-layer removal ahead of side inlets. A turbulent boundary layer was generated on a flat plate, and several wedges were immersed in the boundary layer beneath splitter plates simulating typical side inlet installations.

Parameters investigated included sweep of the splitter plate, wedge included angle, wedge thickness in relation to boundary-layer thickness, and wedge location relative to the leading edge of the splitter plate.

Curves are presented from which may be obtained the pressure drag coefficients of most wedge diverter-type boundary-layer-removal systems. These values are applicable to supercritical inlet operation.

The friction drag coefficients of several wedge diverter-type boundary-layer-removal systems were determined at Mach number 3.16. It was observed that the friction drag of those configurations may constitute a major portion of the total drag of the removal system.

## INTRODUCTION

Various means for improving the performance of side inlets by eliminating the influx of body surface boundary layer include different types of boundary-layer scoop and wedge diverter systems placed beneath the inlet. Among the requirements for an effective boundary-layer-removal system are that it prevent the boundary layer from entering the inlet, that it not generate undesirable disturbances ahead of the inlet, and that it not incur excessive drag. Since any drag accompanying

boundary-layer removal tends to offset the gains in thrust produced by improved inlet performance, any realistic evaluation of side inlet performance with boundary-layer removal must account for the removal drag in determining the net thrust.

The majority of published research on boundary-layer control for side inlets considers scoop systems which duct the boundary-layer air aboard the aircraft. In many situations, however, it may be desired merely to deflect the boundary layer around the inlet by means of a wedge diverter-type system. Although little data on the effectiveness of wedge diverter systems have been published (see refs. 1 and 2), existing information (largely unpublished) indicates that care must be exercised in selecting a particular combination of wedge angle and position under the inlet to prevent the formation of a detached shock wave which deflects excessive boundary-layer flow into the inlet.

The drags associated with a boundary-layer-diverter system include the pressure drag on the wedge faces and the friction drag on all surfaces involved in deflecting the boundary-layer flow. While it is also possible that additional pressure and friction drags due to the diverted flow around the inlet may exist on surfaces downstream of the inlet, these forces evidently depend upon the inlet and body configuration and are not amenable to generalization. Furthermore, even the pressure and friction drags associated with the diverter system itself cannot be predicted analytically because of the nonuniformity of the diverted flow.

The purpose of this experimental investigation was to determine the pressure drag coefficients of a number of boundary-layer wedge diverter systems for a simulated side inlet operating supercritically. It was found in reference 1 that the wedge diverter pressure drag coefficient varied with inlet mass-flow ratio because the diverted flow was influenced by the external shock structure and the resultant inlet flow spillage; however, it was not deemed feasible in this investigation to simulate conditions peculiar to inlet operation at reduced mass flow, since those conditions are evidently functions of specific inlet geometry.

Tests were conducted at Mach numbers of 1.88 and 3.16 in the 18- by 18-inch tunnels and at Mach number 3.83 in the 24- by 24-inch tunnel at the NACA Lewis laboratory. The simulated diverter systems were mounted in the turbulent boundary layer of a flat plate.

In addition to the pressure drag coefficients obtained, an attempt was made to determine the total drag and friction drag coefficients for certain configurations at Mach number 3.16.

Where possible, the wedge diverter-system drags determined in these tests are compared with scoop removal-system drags obtained in other investigations.

## SYMBOLS

| | |
|---|---|
| $a_w$ | wedge included angle, deg |
| $C_p$ | static-pressure coefficient, $\frac{p_w - p_0}{q_0}$ |
| $C_{D_f}$ | friction drag coefficient |
| $C_{D_p}$ | pressure drag coefficient, $\int_0^1 C_p d(x/c)$ |
| $C_{D_t}$ | total drag coefficient, $C_{D_f} + C_{D_p}$ |
| c | wedge length, in. |
| d | width of wedge base, 3.92 in. |
| h | wedge height, in. |
| $h/\delta$ | dimensionless wedge height parameter |
| $l$ | axial distance measured from splitter plate leading edge to wedge apex, in. |
| $l/d$ | dimensionless wedge axial position parameter |
| M | Mach number |
| p | static pressure |
| q | dynamic pressure, $\frac{\gamma p M^2}{2}$ |
| $V/V_0$ | ratio of velocity in boundary layer to free-stream velocity |
| x | axial distance measured from wedge tip, in. |
| y | distance above surface of flat plate, in. |
| z | lateral distance from model center line, in. |

$\gamma$ ratio of specific heats, 1.40

$\delta$ boundary-layer thickness, in.

$\delta^*/\theta$ boundary-layer form factor, displacement thickness/momentum thickness

$\Phi$ splitter plate sweep angle, deg

Subscripts:

w wedge

0 free-stream conditions 1/2 in. upstream of splitter plate

## APPARATUS

Boundary-layer-diverter systems. - The simulated side inlet boundary-layer-diverter system and the parameters investigated are shown schematically in figure 1. These parameters include (1) wedge angle, (2) ratio of wedge thickness to boundary-layer thickness, (3) wedge axial position with respect to the leading edge of the splitter plate, and (4) sweep of the splitter plate leading edge. Four of the five different wedge types employed had straight sides with included apex angles of 16°, 28°, 62°, and 180°. The fifth wedge type had an included apex angle of 26.4°, but its sides were concavely contoured in the form of elliptical arc segments.

A splitter plate was mounted on top of each wedge configuration to simulate the floor of a side inlet. Splitter plates having both unswept and swept leading edges were employed at Mach numbers 1.88 and 3.83, while at Mach 3.16 configurations having a swept splitter plate and no splitter plate were investigated. The sweep angles corresponded to the conical shock angles for 22.4°, 29.2°, and 30° half-angle cones at Mach numbers 1.88, 3.16, and 3.83 and were approximately 47.5°, 51°, and 53°, respectively. The top surface of every splitter plate leading edge was beveled 11.3° in the stream direction to provide a sharp edge. This angle was small enough to prevent shock detachment at these free-stream Mach numbers except for the swept configurations at Mach 1.88. In practice, any bevel employed to thicken the splitter plate for structural purposes might actually be on the underside of the plate.

Provision was made for installing each wedge type in one or more rearward positions with respect to the splitter plate leading edge. The position of the splitter plate leading edge was always maintained 14.5 inches (3.70 splitter plate widths) downstream of the boundary-layer plate leading edge.

[redacted]

Instrumentation. - Wedges were instrumented with static-pressure orifices at regular intervals along one wedge face. Pressures at these stations were indicated on vacuum reference multimanometer boards using tetrabromoethane at Mach number 1.88 and butyl phthalate at Mach numbers 3.16 and 3.83.

In the investigation at Mach number 3.16 a row of static-pressure orifices was installed in the boundary-layer plate beneath the swept splitter plate leading edge and side to assist in the determination of local momentum profiles from total-pressure and flow-angularity surveys. Two movable total-pressure probes were employed in these surveys.

Boundary-layer and free-stream flow characteristics. - Test-section total pressure in each tunnel was essentially atmospheric, while test-section total temperature was 150° F at Mach numbers 1.88 and 3.16 and 200° F at Mach number 3.83.

A strip of carborundum grit 1 inch in width extending across the boundary-layer plate 1/2-inch from the leading edge caused turbulent transition ahead of the diverter system. A total-pressure survey of each boundary layer in a vertical plane through the plate longitudinal center line was made 1/2-inch upstream of the diverter system leading edge station with the diverter system removed. The measured boundary-layer-velocity profiles are presented in figure 2; boundary-layer characteristics of interest as well as the test-section free-stream Reynolds numbers are presented in the following table:

| Free-stream Mach number, $M_0$ | Boundary-layer thickness, $\delta$, in. | Boundary-layer form factor, $\delta^*/\theta$ | Reynolds number per foot |
|---|---|---|---|
| 1.88 | 0.225 | 2.83 | $3.24\times10^6$ |
| 3.16 | .255 | 5.98 | 1.71 |
| 3.83 | .187 | 8.26 | 1.06 |

Test procedure. - At each test Mach number the wedge thickness ratio $h/\delta$ and the wedge axial position parameter $l/d$ were varied systematically for each wedge - splitter plate configuration investigated. The static-pressure coefficient at each orifice station on a wedge face was computed from the equation $C_p = \frac{p_w - p_0}{q_0}$, where $p_w$ was the average static pressure in the vertical pressure profile at that station. The pressure drag coefficient, based on wedge projected frontal area, was computed from the equation

$$C_{D_p} = \int_0^1 C_p \, d\left(\frac{x}{c}\right)$$

Flow-angularity and total-pressure surveys were made in vertical planes at several stations along the splitter plate leading edge and side for certain configurations at Mach number 3.16. These data were used in the determination of total drag and friction drag coefficients for those configurations.

## DISCUSSION OF RESULTS

For most configurations investigated the vertical variation of static pressure at each orifice station was small except perhaps near the wedge apex. Large gradients of average static pressure in the axial direction were frequently encountered, however. Presented in figure 3 are several illustrative axial distributions of static-pressure coefficient $C_p$ obtained at Mach 1.88. The $C_p$ distributions for a given wedge included angle varied with wedge height parameter $h/\delta$ and wedge axial position parameter $l/d$. The greatest variations observed in the investigation, however, were with wedge included angle $a_w$.

The pressure drag coefficients obtained from this investigation are presented in figures 4 to 7 as functions of wedge axial position parameter $l/d$, wedge height parameter $h/\delta$, and free-stream Mach number $M_0$.

Figure 4 presents the observed variations of $C_{D_p}$ with $l/d$ for each value of $h/\delta$ investigated. Plots are presented for each Mach number and splitter plate combination. In general, the largest value of $C_{D_p}$ for each wedge occurred when that wedge was at or near its most forward position; the blunt wedge proved to be an exception. While pressure drag was found to increase with $h/\delta$ for all wedges studied, only small differences were noted for corresponding configurations employing swept and unswept splitter plates at Mach numbers 1.88 and 3.83. Therefore, only swept splitter plate configurations were investigated at Mach number 3.16.

Figure 5 presents cross plots of the data of figure 4 with $C_{D_p}$ plotted as a function of $h/\delta$ at selected values of $l/d$. The increase of $C_{D_p}$ with $h/\delta$ is again clearly observed; also, $C_{D_p}$ increased characteristically with the wedge included angle. It is interesting to observe that the elliptically contoured wedge, which had approximately the same over-all dimensions as the $62^\circ$ wedge, usually incurred larger drag than the $62^\circ$ wedge at Mach numbers 1.88 and 3.83. The blunt, or $180^\circ$, wedge generally exhibited the largest pressure drag, as would be expected. Since the pressure drags for the curved and blunt wedges generally were quite large at Mach numbers 1.88 and 2.93, only the smaller angle wedge configurations were investigated at Mach number 3.16.



[redacted]

The pressure drag coefficients obtained at Mach number 3.16 for the wedges without splitter plate are compared with the data for the comparable swept splitter plate configurations in figure 6. It was found that pressure drag coefficients for the wedges alone were generally smaller than those for the corresponding swept splitter plate configurations. Unpublished studies at North American Aviation Corporation, later confirmed at the Lewis laboratory, have indicated that the performance of side inlets utilizing diverter wedges without splitter plates may prove satisfactory in some cases.



Figure 7 is a cross plot of figure 5, presenting the variation of $C_{D_p}$ with free-stream Mach number for selected combinations of $h/\delta$ and $l/d$. Complete curves were possible only for the smaller angle wedges using the swept splitter plate. However, data points for the curved and 180° wedges obtained with the unswept splitter plate at Mach numbers 1.88 and 3.83 are included. For small values of $l/d$ the drag coefficient $C_{D_p}$ decreased with increasing Mach number. For larger values of $l/d$, however, $C_{D_p}$ was found frequently to increase between Mach numbers 1.88 and 3.16, particularly at the larger values of $h/\delta$. Unpublished data from the Lewis laboratory 8- by 6-foot supersonic tunnel have shown a similar pressure drag coefficient trend between Mach numbers 1.5 and 2.0.

On figure 7 are also plotted values of wedge pressure drag coefficient for 62° wedge swept splitter plate configurations at $l/d = 0$ actually employed as side inlet boundary-layer-diverter systems at Mach numbers 1.88 and 2.93. These values, which are applicable only to supercritical inlet operation, were obtained from cross plots of data presented in reference 1. Although these pressure drag coefficients are greater than those for the equivalent configurations in the present investigation, good agreement of the two sets of data was obtained at large values of $h/\delta$. Static pressures on the downstream portions of the wedges placed beneath the inlets were found to be greater than those in the same regions of comparable configurations in the present investigation, especially at small values of $h/\delta$. These discrepancies in wedge static pressures and pressure drag coefficient are in part due to the effects on the diverted flow caused by (1) disturbances from the inlet spike and cowl, (2) the supercritical spillage of these inlets, and (3) a slight bevel on the underside of the inlet configuration splitter plate leading edges rather than on the upper side as in the present investigation.

Friction drag and total drag coefficients at Mach number 3.16. - An effort was made to determine friction drag and total drag coefficients of several swept splitter plate configurations at Mach number 3.16. For this purpose total-pressure and flow-angularity surveys were performed

[redacted]

in several vertical planes along the splitter plate leading edge and side, although tunnel limitations restricted these surveys to the large angle wedges in forward positions. These surveys, together with static pressures on the boundary-layer plate along the surveyed edges of the splitter plate, were used to determine the streamwise components of the entering and leaving total momentum of the flow diverted beneath the splitter plate. The total momentum decrement, representing the total drag of the configuration, consisted of the wedge pressure drag and the friction drag of the surfaces wetted by the diverted flow. Thus both components of the total drag coefficient were obtained and are presented in figure 8. It is estimated that these total drag coefficients are accurate within $\pm 10$ percent, and the friction drag coefficients, within $\pm 15$ percent of the indicated values.

3150

At all values of $h/\delta$ and $l/d$ investigated for both wedges, the friction drag coefficient was found to be a large part of the total drag coefficient. At $h/\delta$ of unity the friction drag coefficient for the $28^\circ$ wedge configuration is approximately 3/4 of the total drag coefficient. For the $62^\circ$ wedge configuration the friction drag coefficient represents the greater portion of total drag coefficient at low values of $h/\delta$, but unlike that of the $28^\circ$ wedge configuration, makes the smaller contribution at larger values of $h/\delta$, especially at large values of $l/d$. For both wedge types the friction drag coefficient increases with increasing $h/\delta$ at small values of $l/d$.

A comparison of some of the wedge diverter-system drags obtained in the present investigation and the drag associated with boundary-layer removal by a scoop is presented in figure 9. Compared are the total drags obtained at Mach number 3.16 for the $28^\circ$ and $62^\circ$ wedge configurations at $l/d$ of zero, with no inlet present, and the drag of a swept leading edge scoop beneath a side inlet operating at Mach number 2.93 (see ref. 1). The scoop drag is that due to the momentum change of the scoop mass flow between the scoop entrance and an assumed sonic discharge nozzle. Experimentally obtained values of scoop mass flow and total-pressure recovery corresponding to critical inlet operation were used in the momentum computations. The swept-scoop drag was considerably less than the $62^\circ$ wedge diverter-system drag for values of $h/\delta$ less than 1.2. While the $28^\circ$ wedge diverter-system drag was less than that for the $62^\circ$ wedge diverter system for values of $h/\delta$ less than about 1.0, it was nevertheless greater than the scoop drag except at very low values of $h/\delta$.

Visual flow observations. - A consideration of the disturbances initiated by the wedge diverter configurations is necessary inasmuch as one requirement for an effective boundary-layer-removal system is that it not disturb the flow into the side inlet. Any disturbances resulting from the diverter wedge shock and its interaction with the boundary layer may affect the flow into the inlet if these disturbances extend ahead of the splitter plate leading edge.

[redacted]

Some degree of boundary-layer separation ahead of the unswept splitter plate configurations investigated at the three smallest values of $h/\delta$ was always present at Mach number 1.88, and, to a lesser extent, at the smallest value of $h/\delta$ investigated at Mach number 3.83. The primary reason for this separation at low values of $h/\delta$, particularly at Mach 1.88, was shock detachment from the 11.3° splitter plate leading edge bevel. Separation was most pronounced, however, when wedge $l/d$ was zero and wedge included angle was large, for then the wedge detached bow wave added to the splitter plate disturbance. Although the swept splitter plate shock was detached at Mach number 1.88, there was no evidence of boundary-layer separation at these low $h/\delta$ values except for wedge $l/d$ of zero. Figure 10 presents schlieren photographs of typical low $h/\delta$ configurations at Mach number 1.88 for both splitter plates. These photographs are also representative of the observations at Mach numbers 3.16 and 3.83.

Boundary-layer separation ahead of the unswept splitter plate configurations at larger values of $h/\delta$ was observed at Mach numbers 1.88 and 3.83 only at wedge $l/d$ of zero, except for the 180° wedge configuration, which caused separation even at moderately large values of wedge $l/d$ because of the strong bow wave. Reflecting shock patterns were established beneath the unswept splitter plate at Mach number 1.88 for large values of $h/\delta$ when there was no boundary-layer separation, but this type of disturbance was not observed at Mach number 3.83. Such shock patterns were never visible beneath the swept splitter plate at any of the three Mach numbers. Representative schlieren photographs are presented in figure 11 for large $h/\delta$ configurations at Mach number 1.88.

It is possible that boundary-layer separation ahead of a wedge configuration had some effect on the wedge pressure drag. However, an examination of figure 4, which compares the pressure drag coefficients for both unswept and swept splitter plate configurations at Mach numbers 1.88 and 3.83, does not show any consistent effect of initial boundary-layer separation on the wedge pressure drag.

The disturbances beneath the splitter plate frequently seen in the schlieren photographs consisted of a bow wave ahead of the wedge and in certain instances a shock pattern resulting from the disturbance at the splitter plate leading edge. By permitting a solution of machinists' layout blue in alcohol to flow onto the boundary-layer plate through a forward plate static-pressure orifice during the test, traces of these waves, as well as some indication of the flow streamlines were obtained as the alcohol evaporated, leaving the blue adhering to the plate surface.

[redacted]

This flow visualization technique, however, has several limitations. It should be pointed out that the fluid traces do not give the exact shock locations, but rather remain somewhat upstream of the true shock location as a result of pressure feedback through the boundary layer at the shock, and that true shock form is probably valid only near the center line of the model inasmuch as the fluid patterns begin to indicate streamlines rather than shock patterns as the shock weakens. Furthermore, in the case of multiple shocks, the fluid often indicated only the upstream shock. This occurred most frequently for configurations utilizing the unswept splitter plate; the pressure rise across the disturbance from the splitter plate leading edge was sometimes sufficient to prevent the fluid from passing through to give indications of further disturbances. However, when alcohol alone was passed through the pressure orifice, it frequently would penetrate the splitter plate disturbance and locate the wedge bow wave. For configurations using the swept splitter plate, often only the wedge disturbance was located since the disturbance from the splitter plate was weak.



Figure 12 presents typical variations of the shock patterns determined from the visual flow technique at Mach number 3.83. Sketches were made at the time of running and represent as nearly as possible the observed patterns. Figures 12(a), (b), and (c) present variations of the shock disturbance field with wedge position, wedge included angle, and splitter plate sweep, respectively. Very little variation of these patterns was noted with $h/\delta$, although there was considerable variation with $l/d$. As the wedge was moved aft, the wedge bow wave tended to separate from the splitter plate disturbance and to move aft with the wedge. This tendency is, of course, beneficial to side inlet operation. Increasing the wedge included angle (fig. 12(b)) was found to push the wedge bow wave upstream.

Actual photographs of some shock disturbance traces at Mach 3.16 are presented in figure 13. It is noted that at $l/d$ of 0 some shock disturbance was always ahead of the splitter plate. This disturbance, however, was considerably reduced as the wedge included angle was reduced. Also, the disturbance could be made to move beneath the splitter plate by increasing $l/d$. Good side inlet performance should therefore be possible using small angle wedge diverters or larger angle wedge diverters at values of $l/d$ great enough to prevent the diverter disturbance from entering the inlet.

## CONCLUDING REMARKS

Graphs are presented from which the pressure drag coefficients of a large number of wedge diverter-type boundary-layer-removal systems for use with side inlets may be estimated. Little difference was found in the pressure drag coefficients of most equivalent unswept and swept

splitter plate configurations. Since the boundary-layer-diverter systems investigated were simplified to the extent that interference effects due to the inlet external shock structure and mass-flow spillage were eliminated, these data are most applicable to supercritical inlet operation at the larger values of wedge height parameter.

Visual studies of the shock disturbances of each configuration seem to indicate that good side inlet performance with wedge diverter-type boundary-layer-removal systems can be obtained if the wedge axial position parameter is large enough to prevent those disturbances from entering the inlet.

This investigation indicates that the friction drag of a wedge diverter system may constitute a major portion of the total drag of the system. It is therefore evident that additional research is needed before a final evaluation of wedge diverter-type boundary-layer removal can be made.

Lewis Flight Propulsion Laboratory
National Advisory Committee for Aeronautics
Cleveland, Ohio, December 22, 1953.

## REFERENCES

1. Piercy, Thomas G., and Johnson, Harry W.: A Comparison of Several Systems of Boundary-Layer Removal Ahead of a Typical Conical External-Compression Side Inlet at Mach Numbers 1.88 and 2.93. NACA RM E53F16, 1953.

2. Valerino, Alfred S., Pennington, Donald B., and Vargo, Donald J.: Effect of Circumferential Locations on Angle of Attack Performance of Twin Half-Conical Scoop-Type Inlets Mounted Symmetrically on the RM-10 Body of Revolution. NACA RM E53G09, 1953.

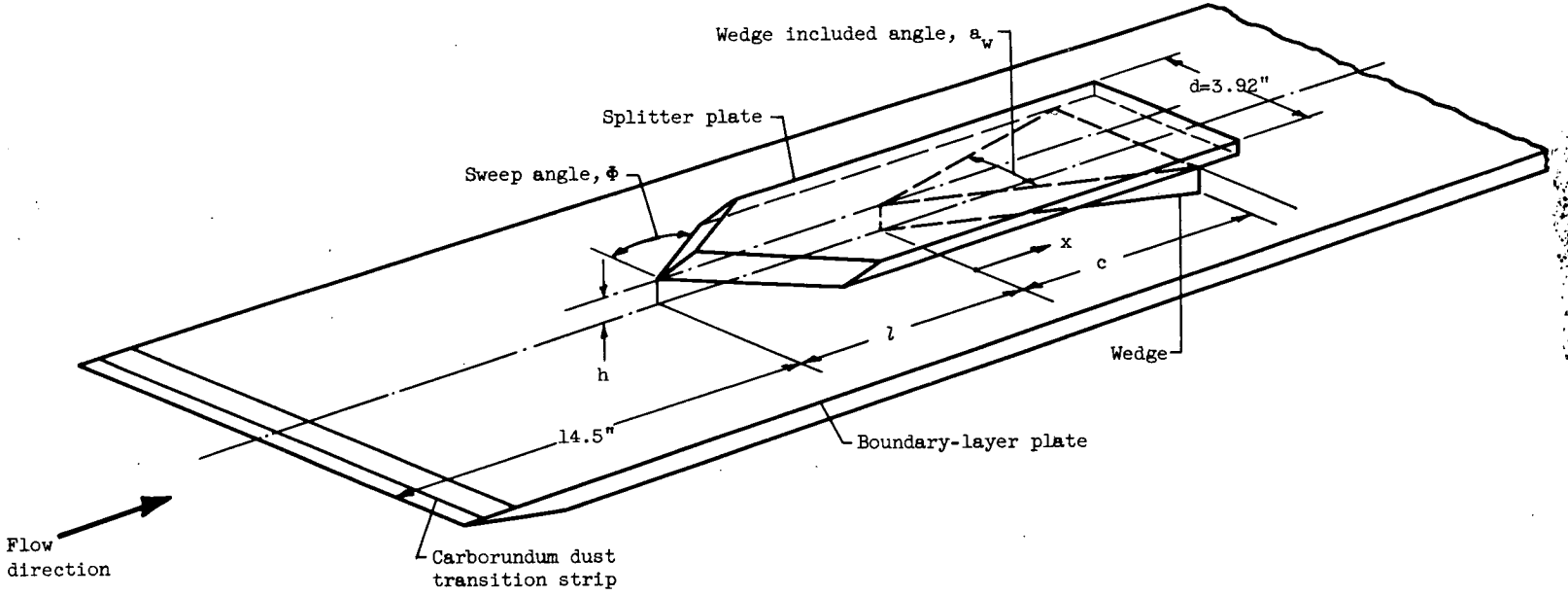


(a) General arrangement.

Figure 1. - Schematic views of wedge diverter model.

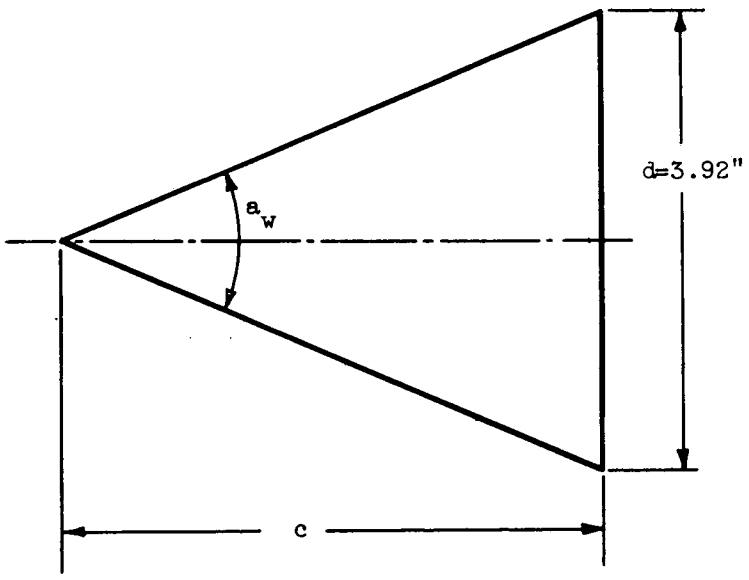


Straight side wedges

| $a_w$, deg | c, in. |
|---|---|
| 16 | 13.94 |
| 28 | 7.84 |
| 62 | 3.26 |
| 180 | 2.25 |

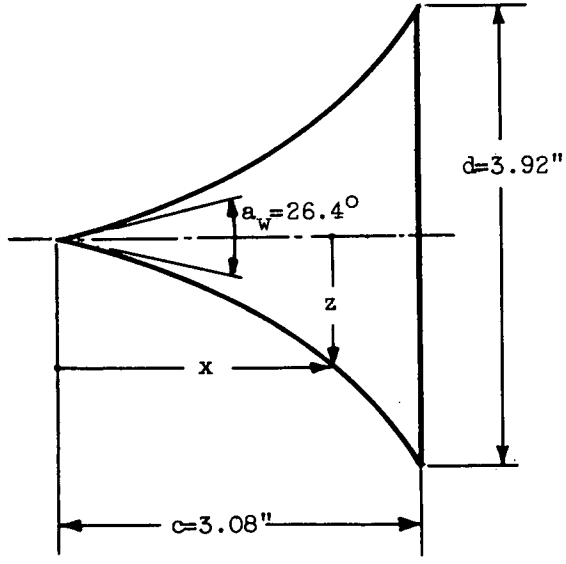


Elliptical contour wedge

| Coordinates, in | |
|---|---|
| x | z |
| 0 | 0 |
| .2 | .047 |
| .6 | .165 |
| 1.0 | .315 |
| 1.5 | .556 |
| 2.0 | .869 |
| 2.5 | 1.280 |
| 3.08 | 1.960 |

(b) Wedge diverter dimensions.

**Figure** 1. - Concluded. Schematic views of wedge diverter model.

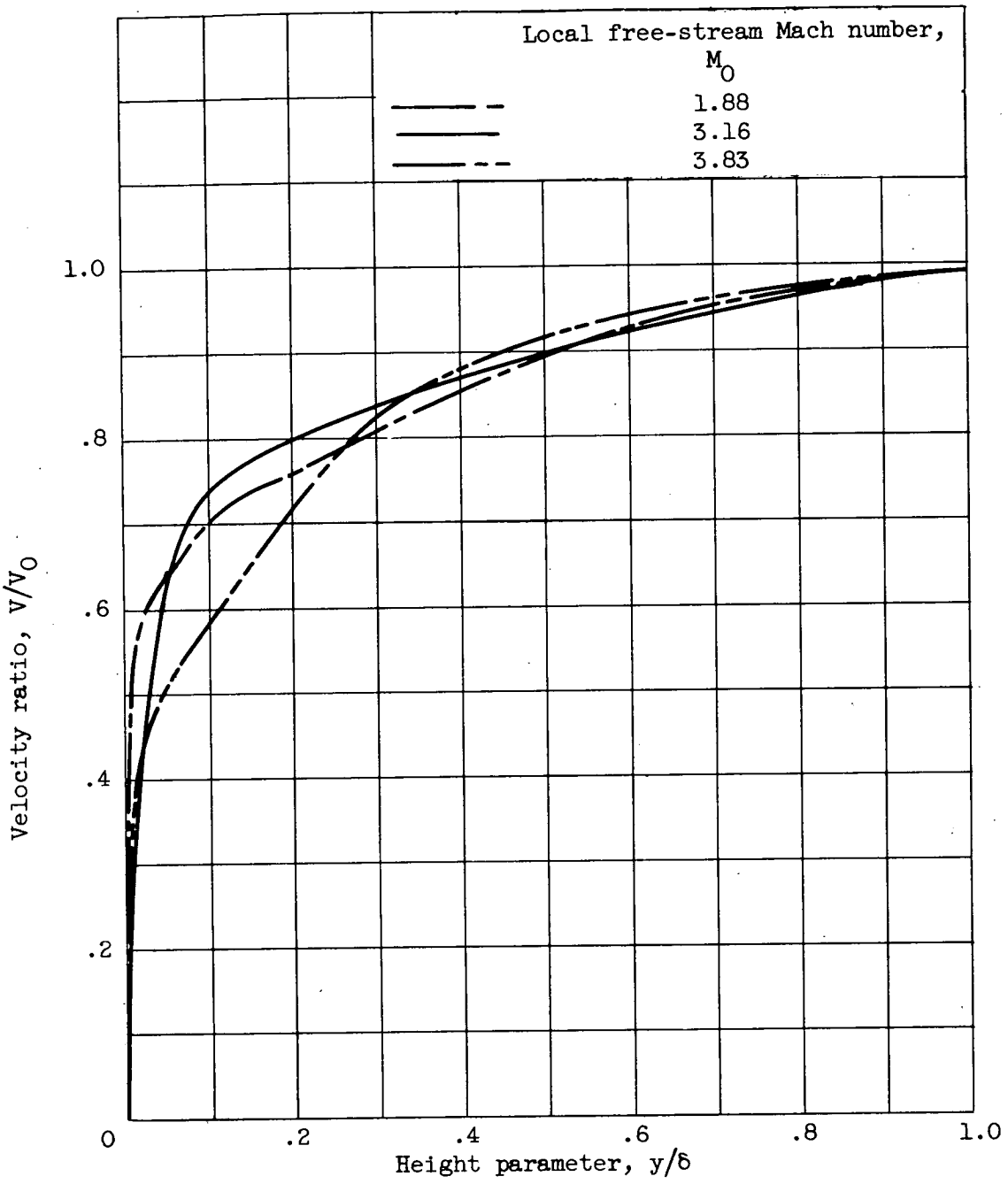


Figure 2. - Boundary-layer-velocity profiles.

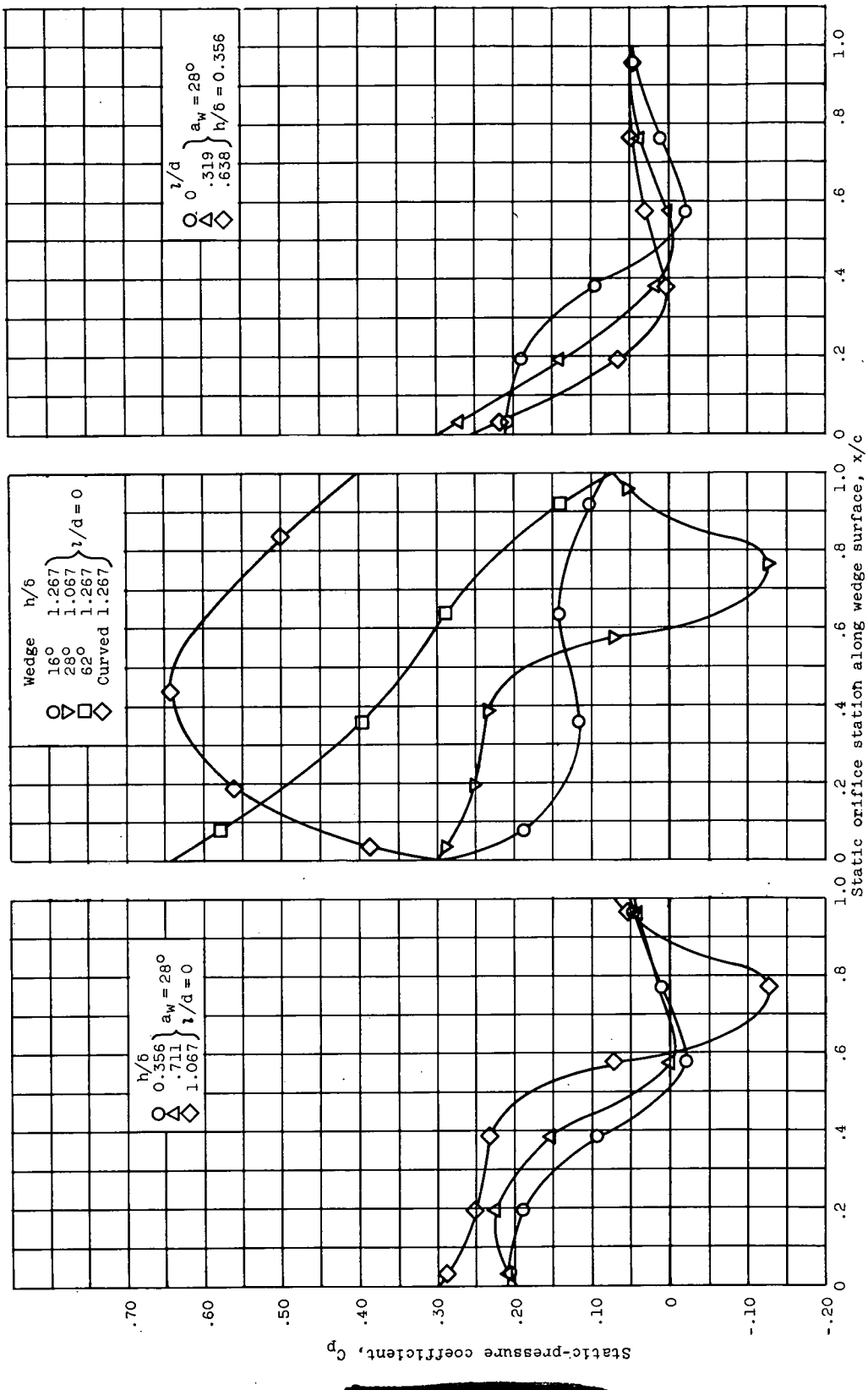


Figure 3. - Illustrative axial distributions of wedge face pressure coefficient for several swept splitter plate configurations at Mach 1.88.

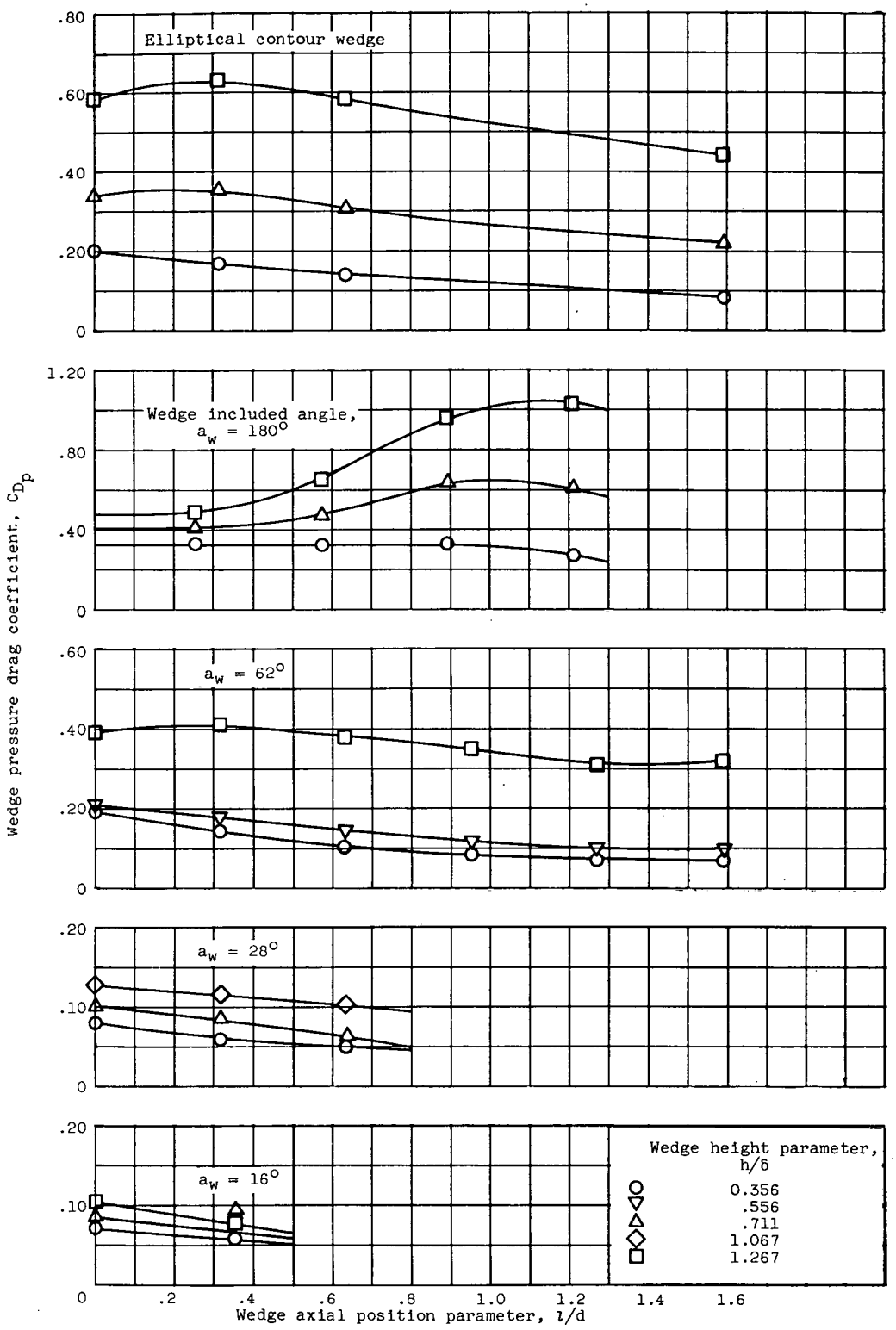


(a) Free-stream Mach number, 1.88; unswept splitter plate.

Figure 4. - Effect of wedge axial position relative to splitter plate on pressure drag coefficient of several wedges.

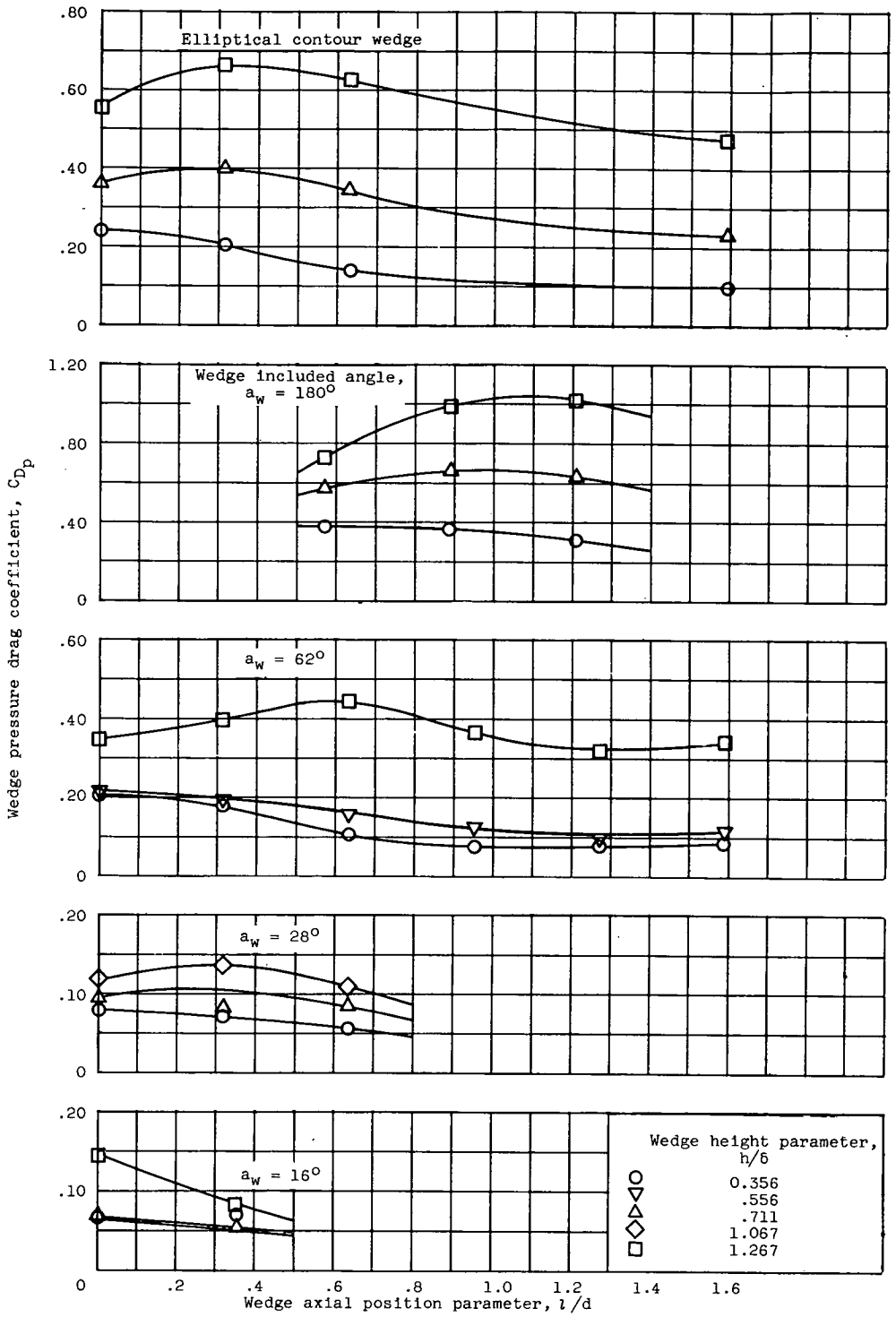


(b) Free-stream Mach number, 1.88; 47.5° swept splitter plate.

Figure 4. - Continued. Effect of wedge axial position relative to splitter plate on pressure drag coefficient of several wedges.

[redacted]

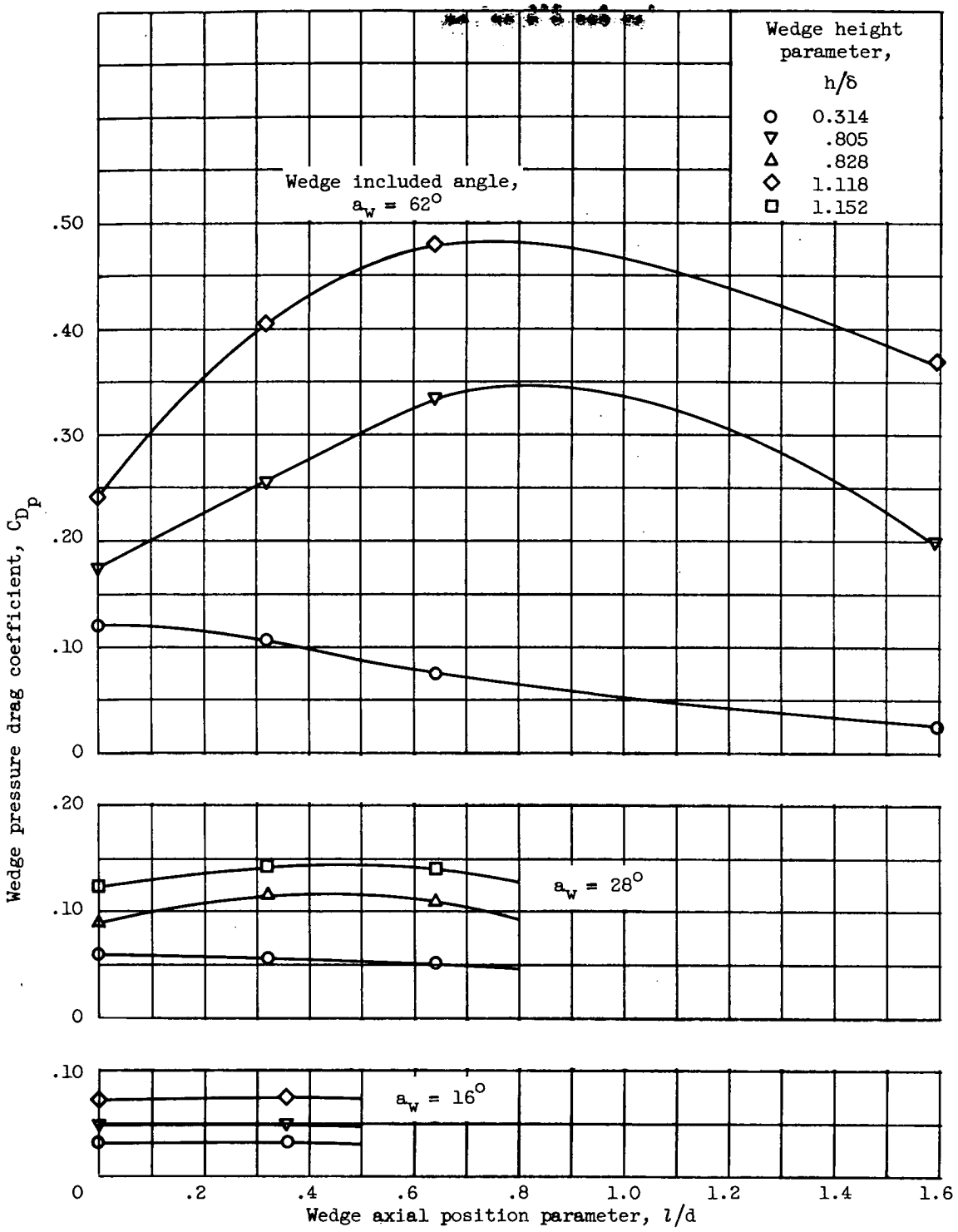


(c) Free-stream Mach number, 3.16; 51.0° swept splitter plate.

Figure 4. - Continued. Effect of wedge axial position relative to splitter plate on pressure drag coefficient of several wedges.

[redacted]

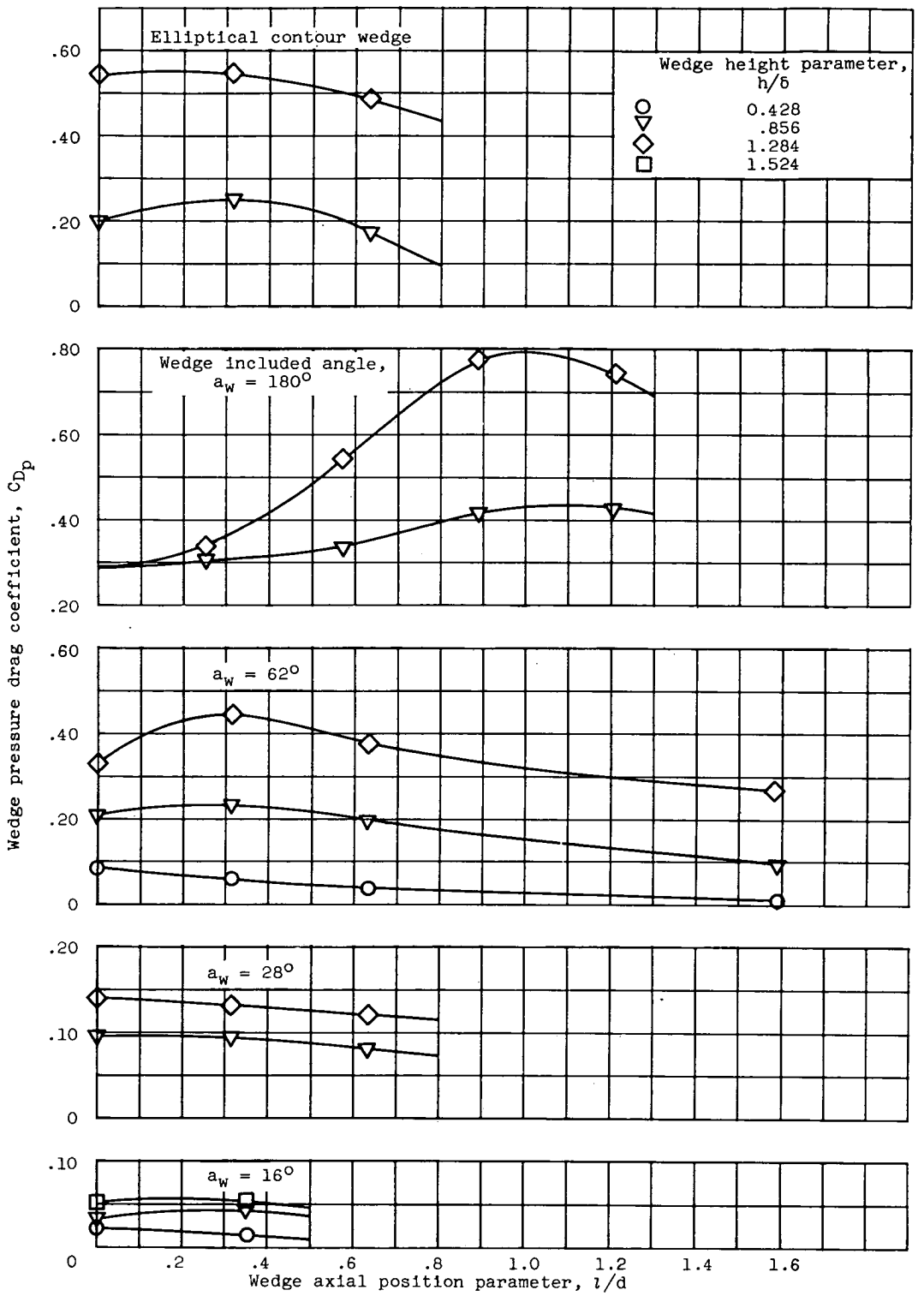


(d) Free-stream Mach number, 3.83; unswept splitter plate.

Figure 4. - Continued. Effect of wedge axial position relative to splitter plate on pressure drag coefficient of several wedges.

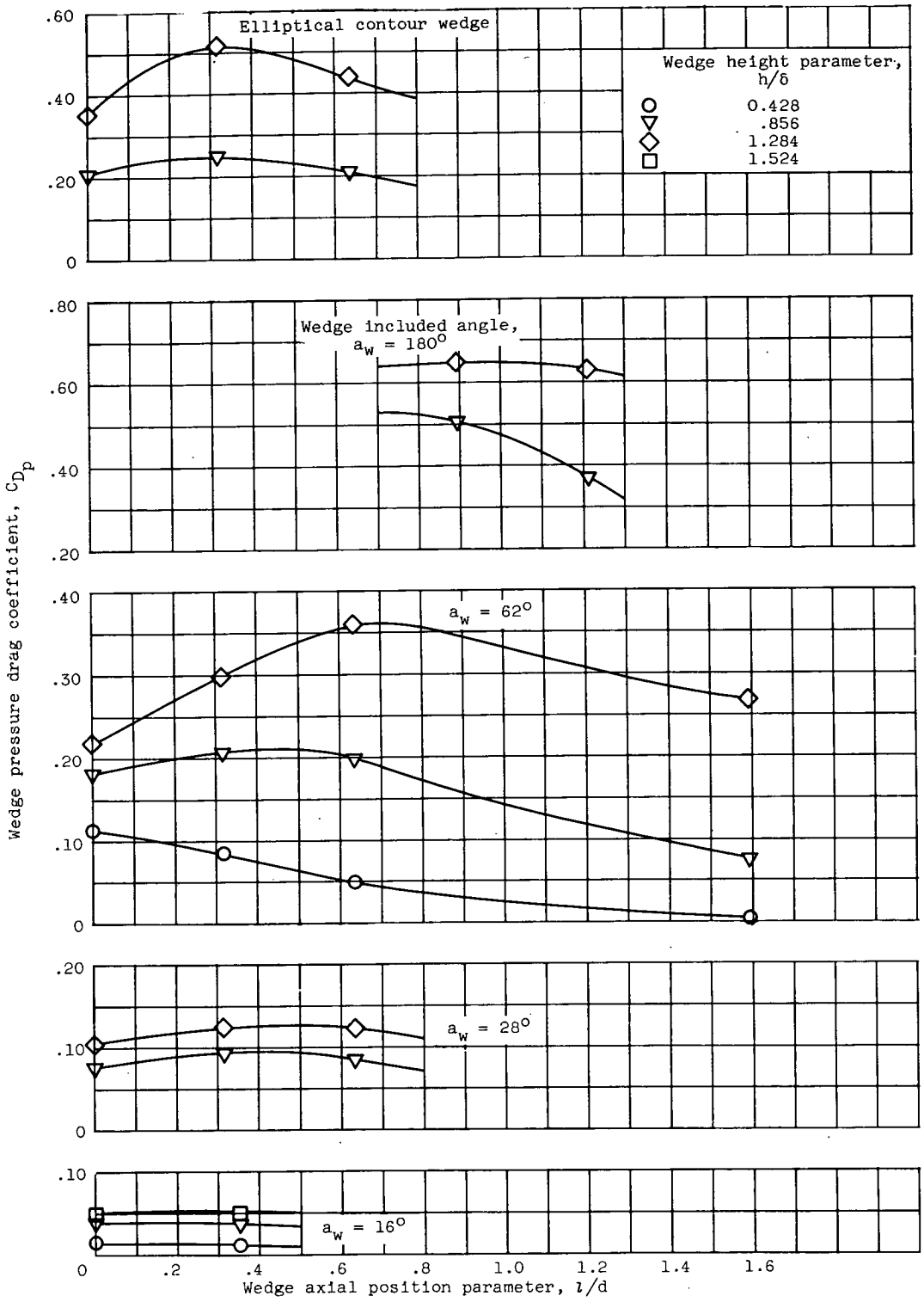


(e) Free-stream Mach number, 3.83; 53.0° swept splitter plate.

Figure 4. - Concluded. Effect of wedge axial position relative to splitter plate on pressure drag coefficient of several wedges.

[redacted]

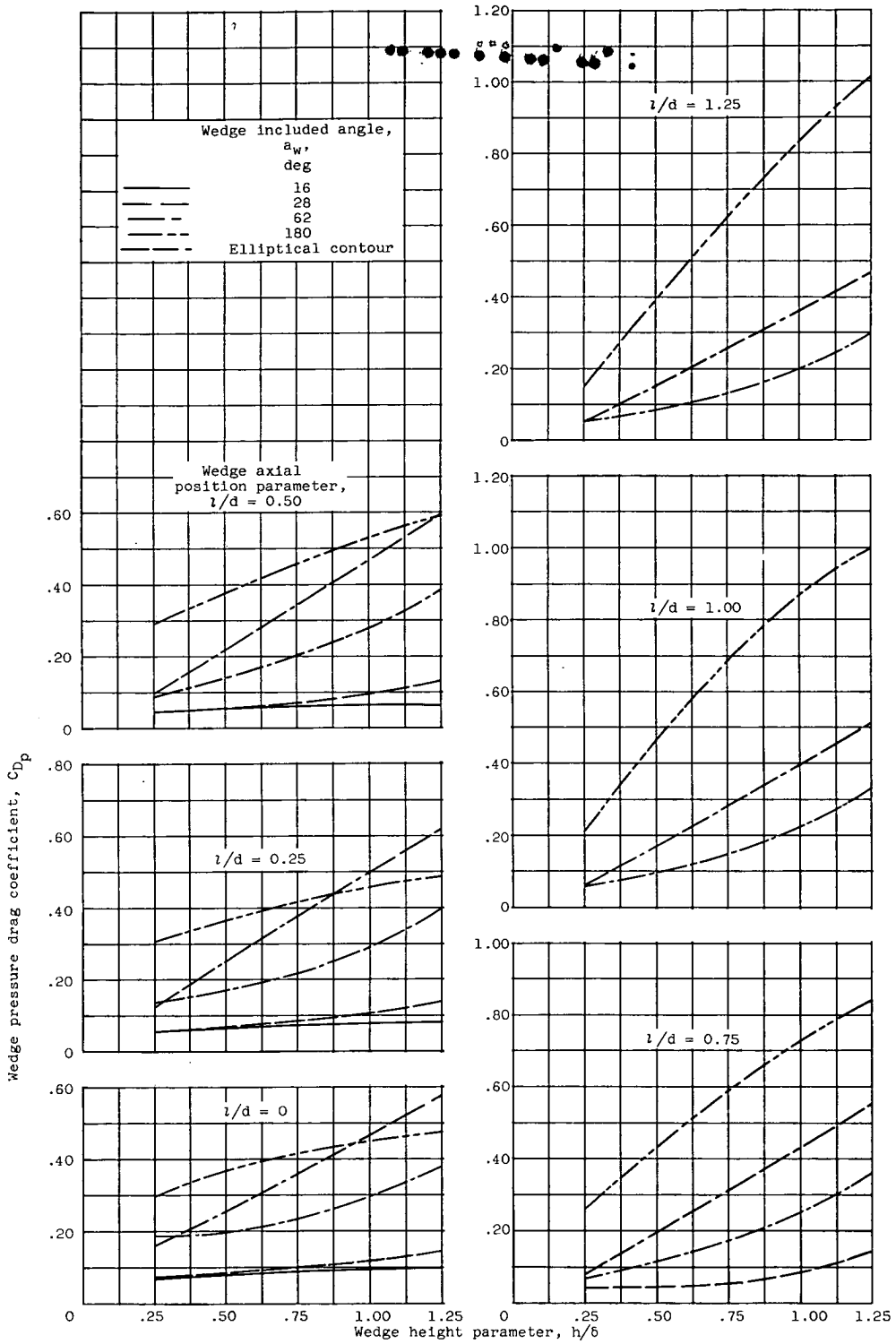


(a) Free-stream Mach number, 1.88; unswept splitter plate.

Figure 5. - Effect of wedge height on pressure drag coefficient of several wedges.

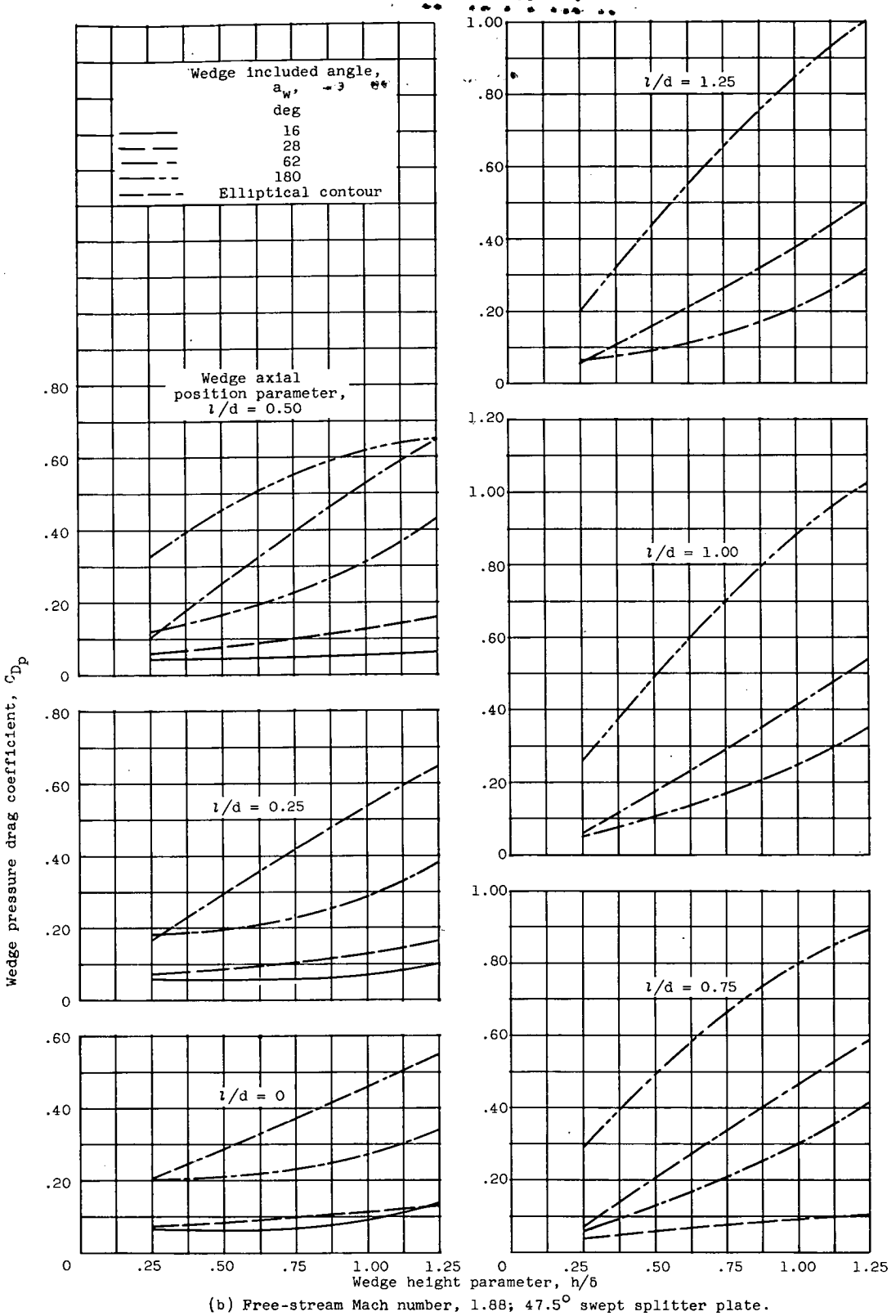


(b) Free-stream Mach number, 1.88; 47.5° swept splitter plate.

Figure 5. - Continued. Effect of wedge height on pressure drag coefficient of several wedges.

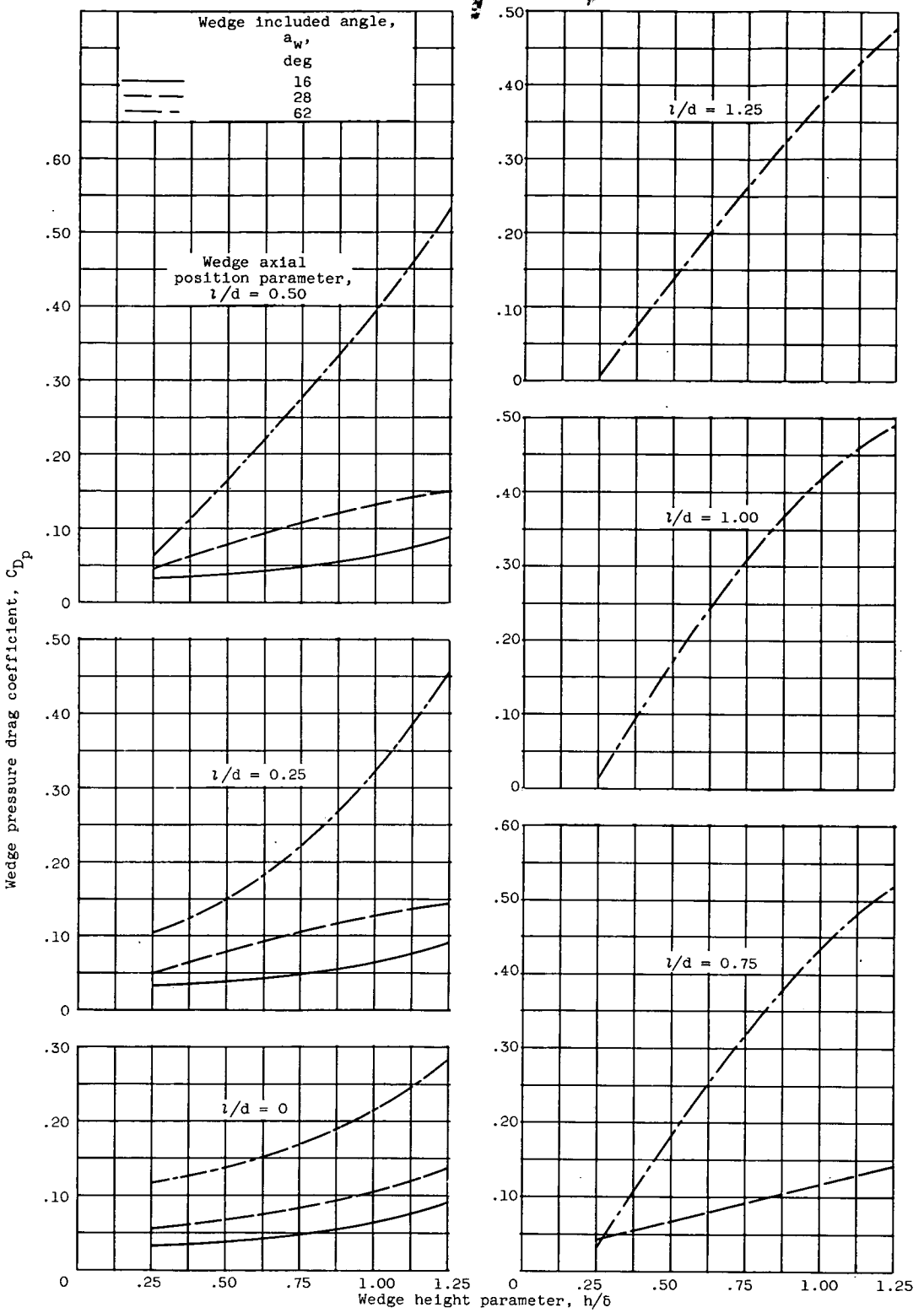


(c) Free-stream Mach number, 3.16; 51.0° swept splitter plate.

Figure 5. - Continued. Effect of wedge height on pressure drag coefficient of several wedges.

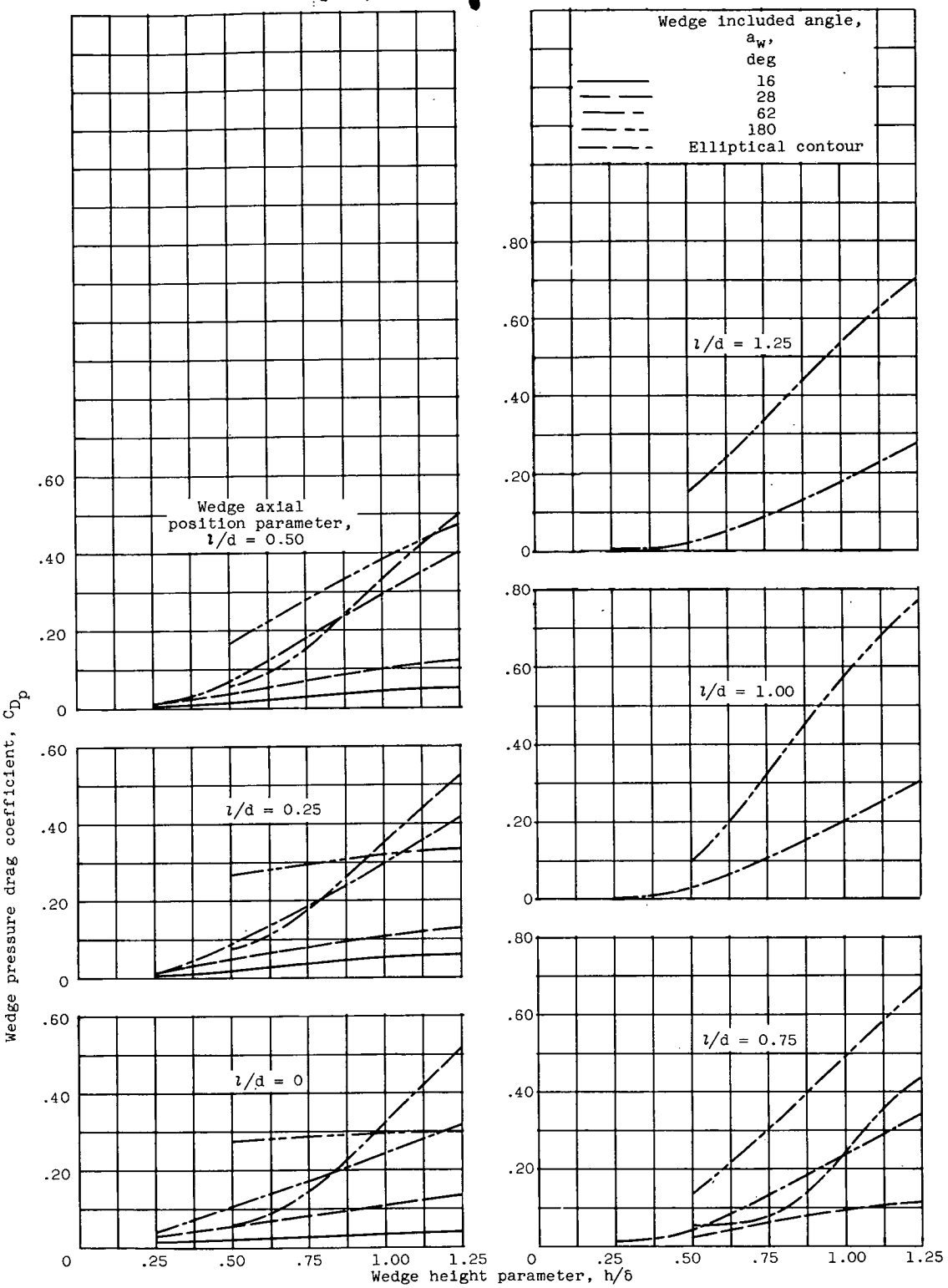


(d) Free-stream Mach number, 3.83; unswept splitter plate.

Figure 5. - Continued. Effect of wedge height on pressure drag coefficient of several wedges.

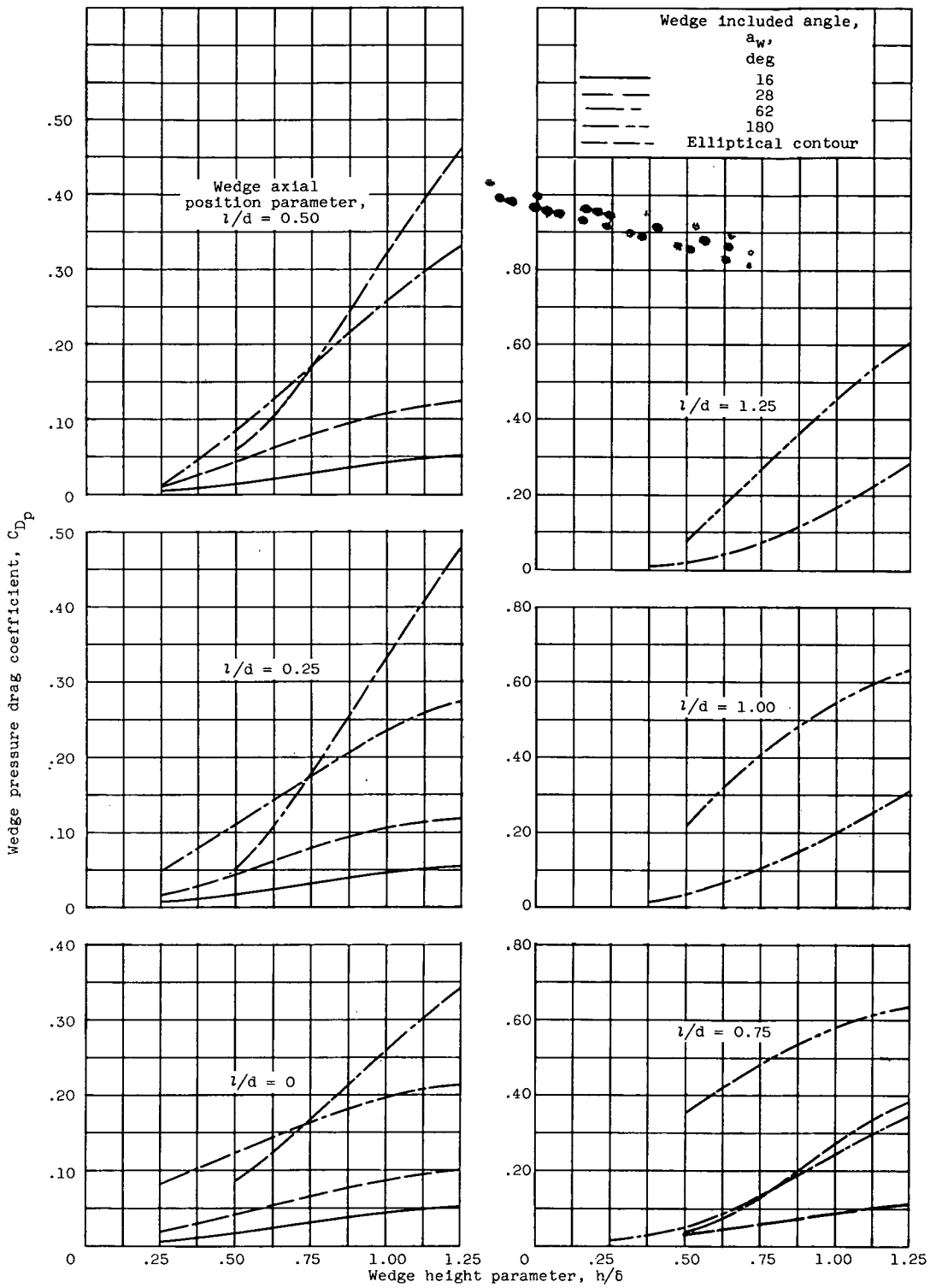


(e) Free-stream Mach number, 3.83; swept splitter plate.

Figure 5. - Concluded. Effect of wedge height on pressure drag coefficient of several wedges.

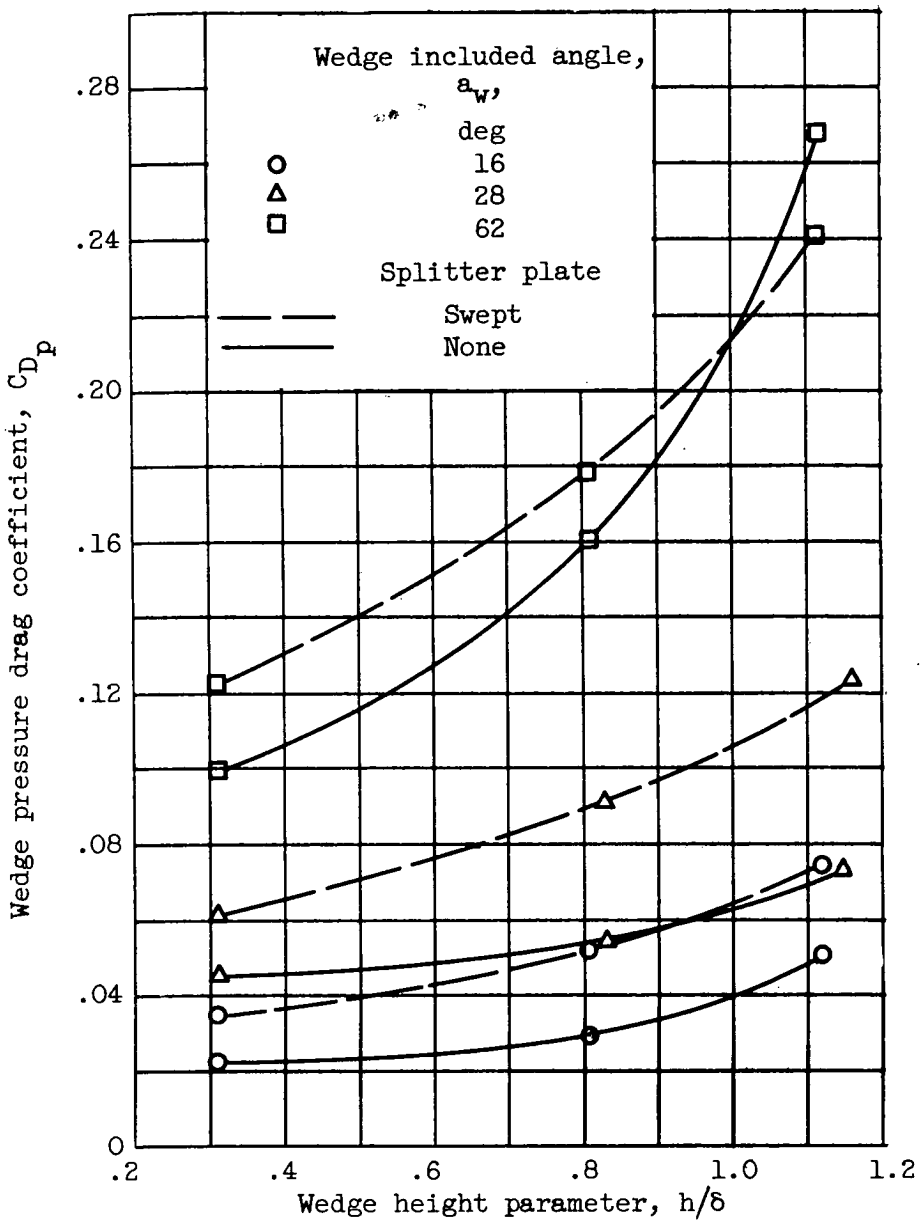


Figure 6. - Comparison at Mach 3.16 of wedge pressure drag coefficients with no splitter plate and with swept splitter plate for wedge axial position parameter of 0.

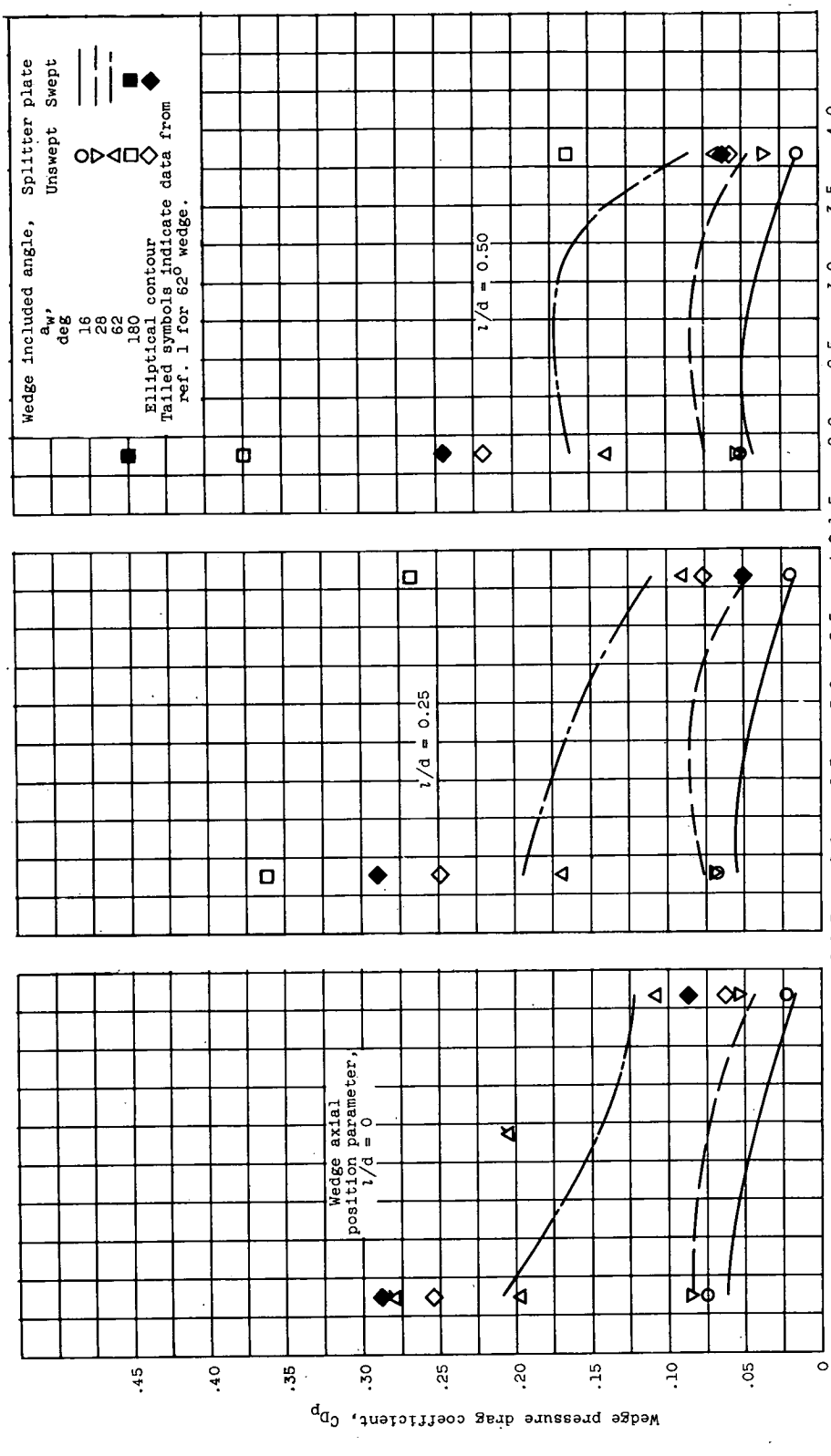


(a) Wedge height parameter, 0.50.

Figure 7. - Variation of wedge pressure drag coefficient with free-stream Mach number.

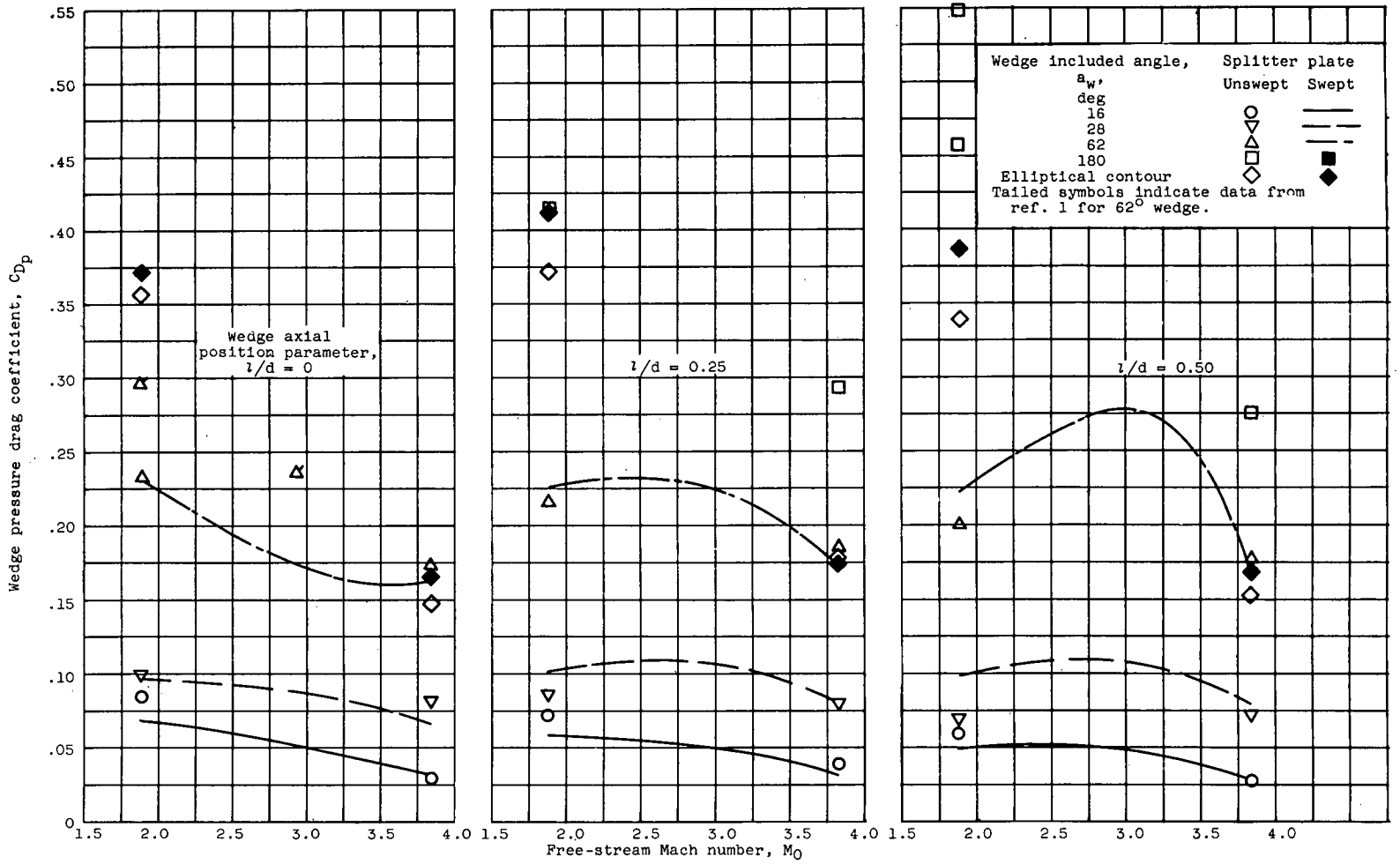


(b) Wedge height parameter, 0.75.

Figure 7. - Continued. Variation of wedge pressure drag coefficient with free-stream Mach number.

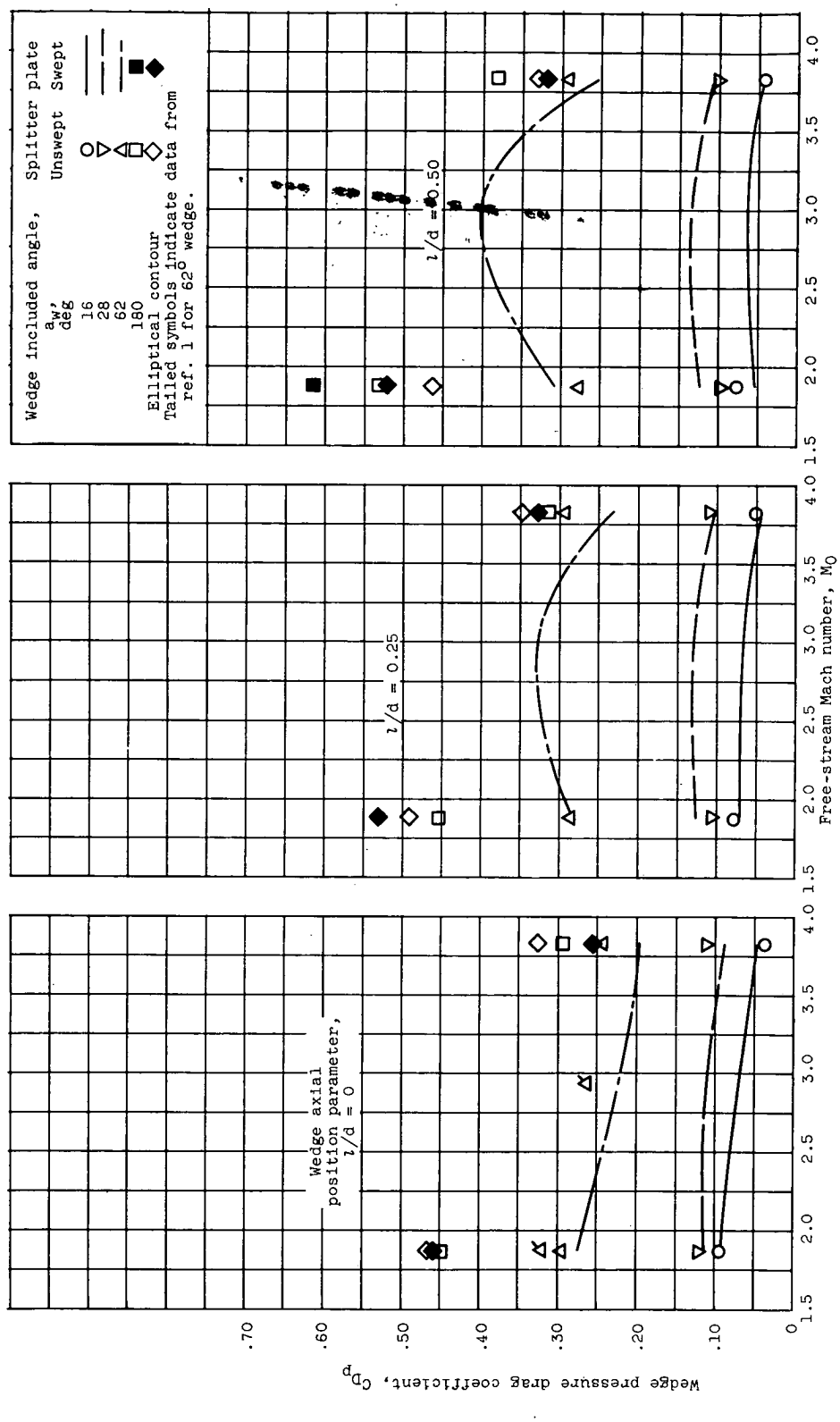


(c) Wedge height parameter, 1.00.

Figure 7. - Continued. Variation of wedge pressure drag coefficient with free-stream Mach number.

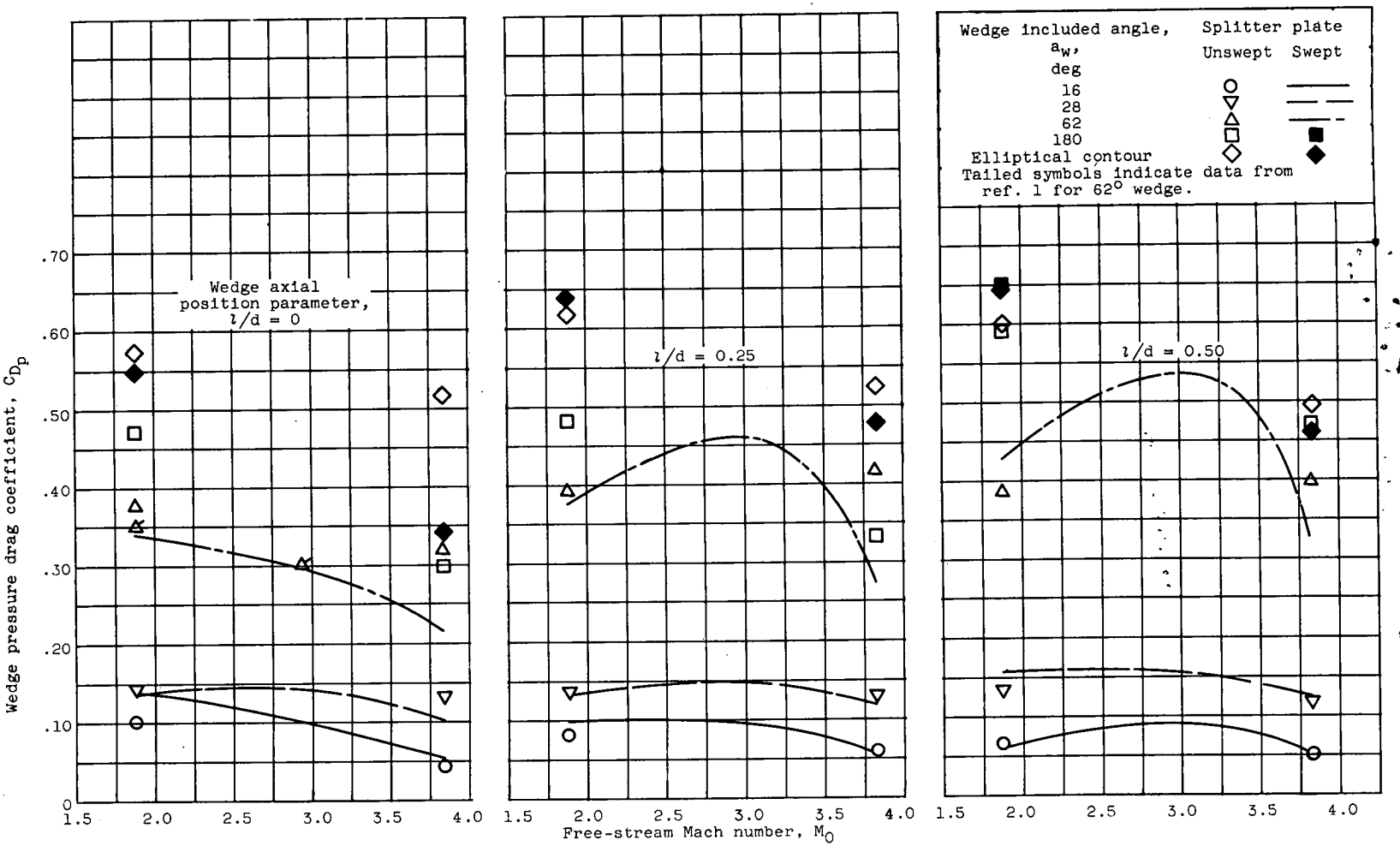


(d) Wedge height parameter, 1.25.

Figure 7. - Concluded. Variation of wedge pressure drag coefficient with free-stream Mach number.

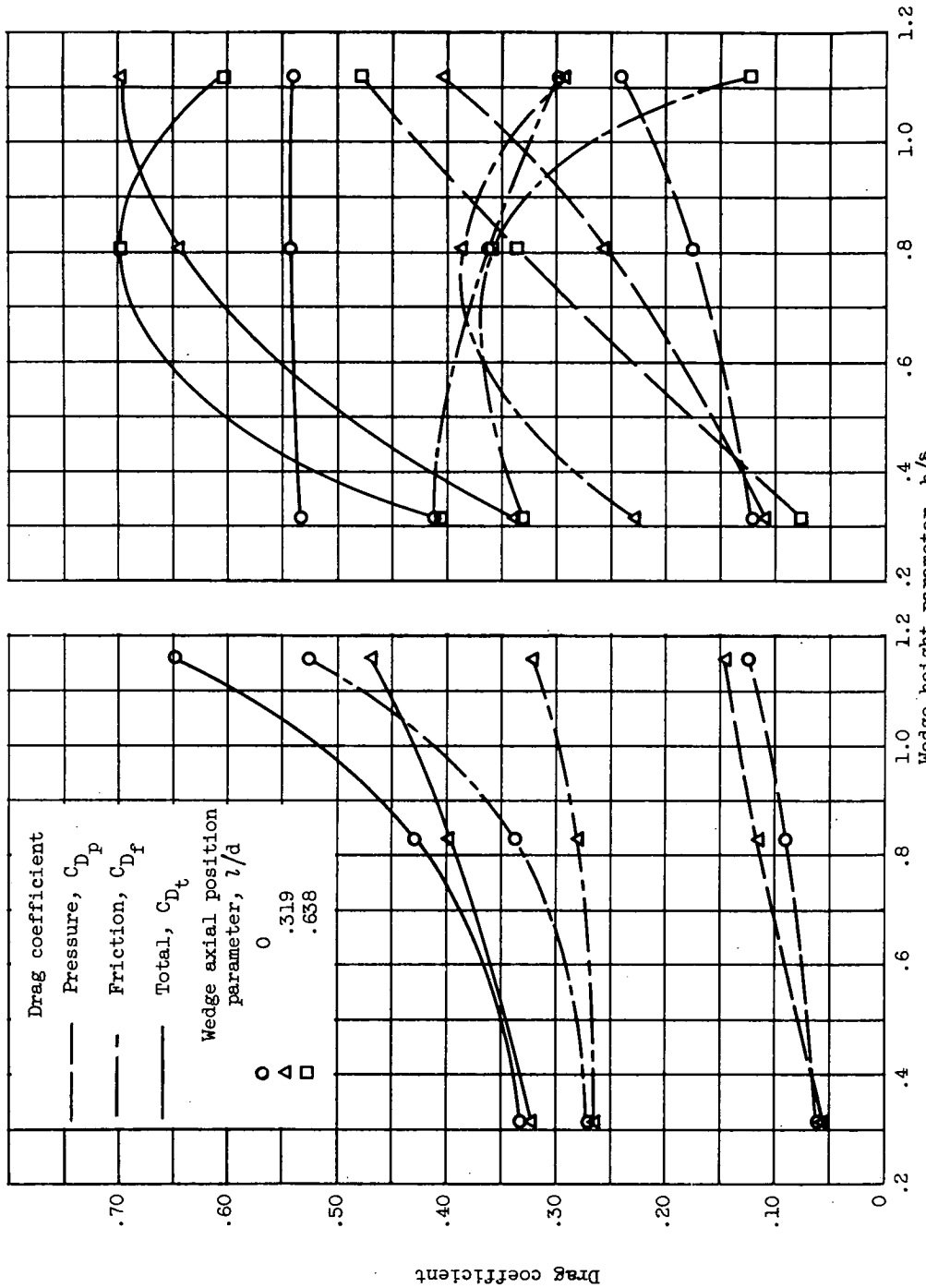


(a) 28° Included angle wedge. (b) 62° Included angle wedge.

Figure 8. - Comparison of pressure, friction, and total drag coefficients for two wedges with swept splitter plate at Mach 3.16.

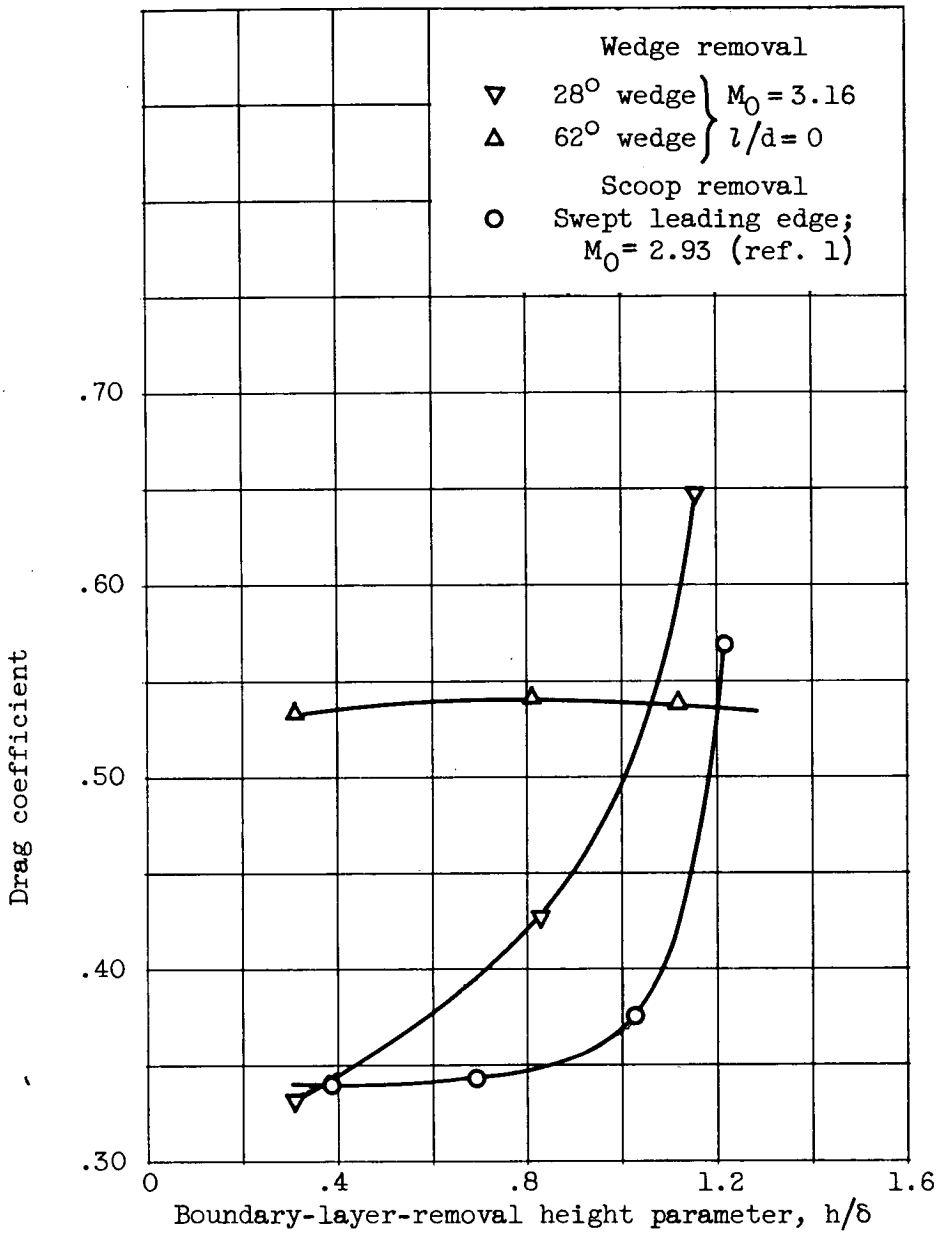


Figure 9. - Comparison of wedge and scoop boundary-layer-removal drags.

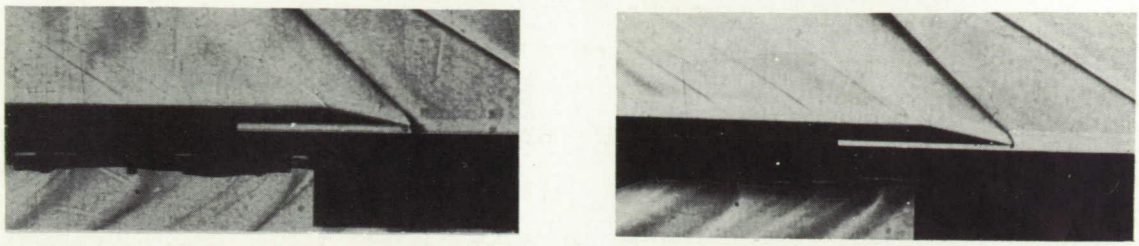

Unswept splitter plate; $l/d = 0.638$

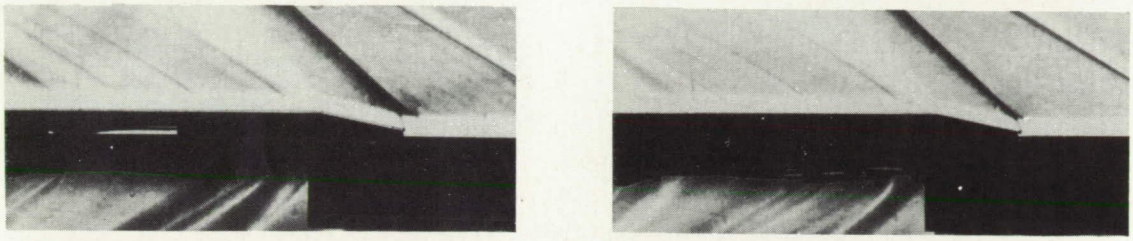

Unswept splitter plate; $l/d = 0$

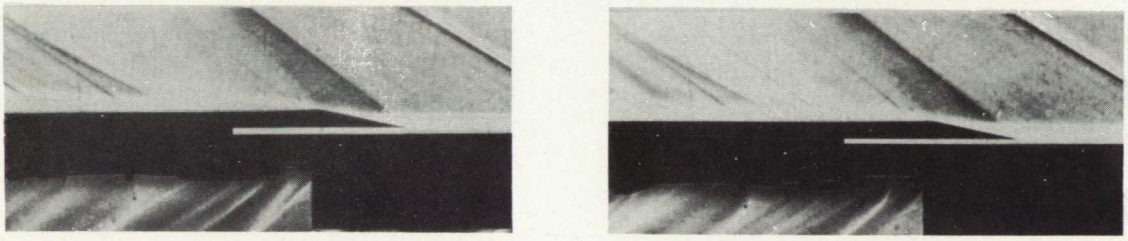

Swept splitter plate; $l/d = 0.638$

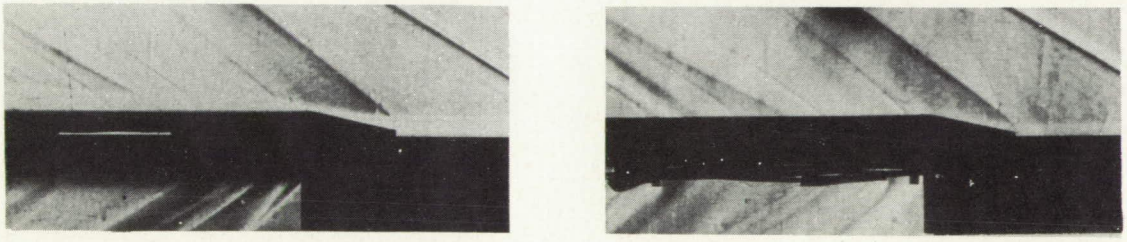

Swept splitter plate; $l/d = 0$ C-34517

(a) $62^{\circ}$ Wedge; $h/\delta = 0.356$. (b) $28^{\circ}$ Wedge; $h/\delta = 0.356$.

Figure 10. - Schlieren photographs at Mach 1.88 and small values of wedge height parameter.

[redacted]

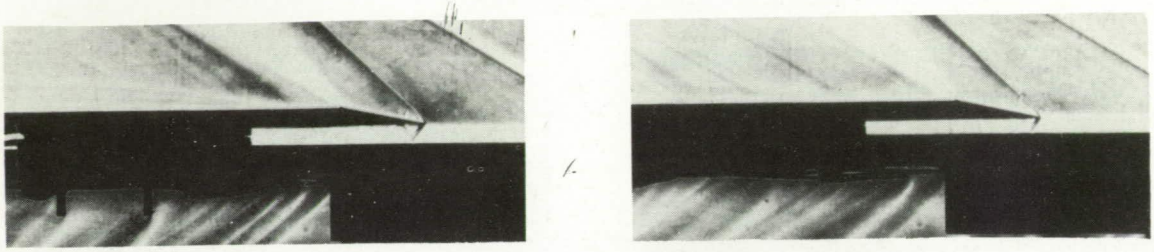

Unswept splitter plate; $l/d = 0.638$

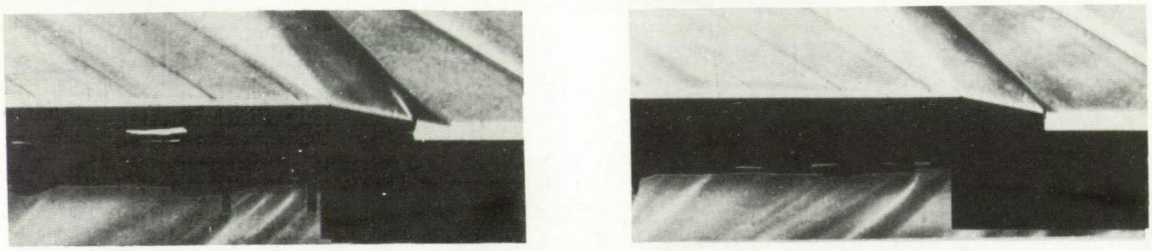

Unswept splitter plate; $l/d = 0$

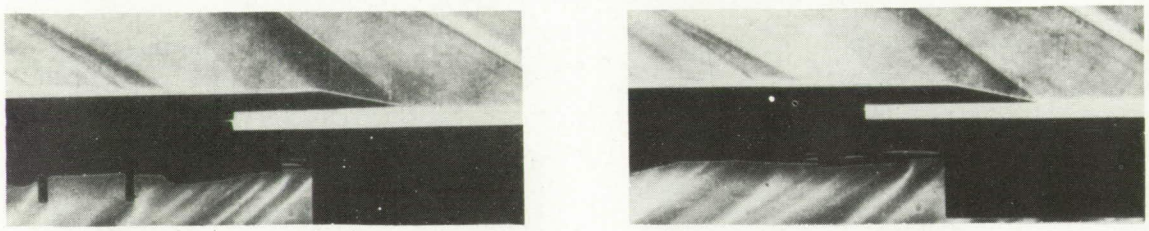

Swept splitter plate; $l/d = 0.638$

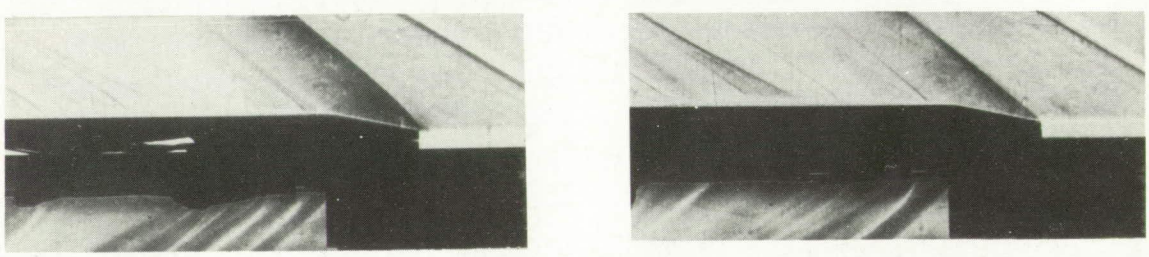

Swept splitter plate; $l/d = 0$ C-34518

(a) 62° Wedge; $h/\delta = 1.267$. (b) 28° Wedge; $h/\delta = 1.067$.

Figure 11. - Schlieren photographs at Mach 1.88 and large values of wedge height parameter.

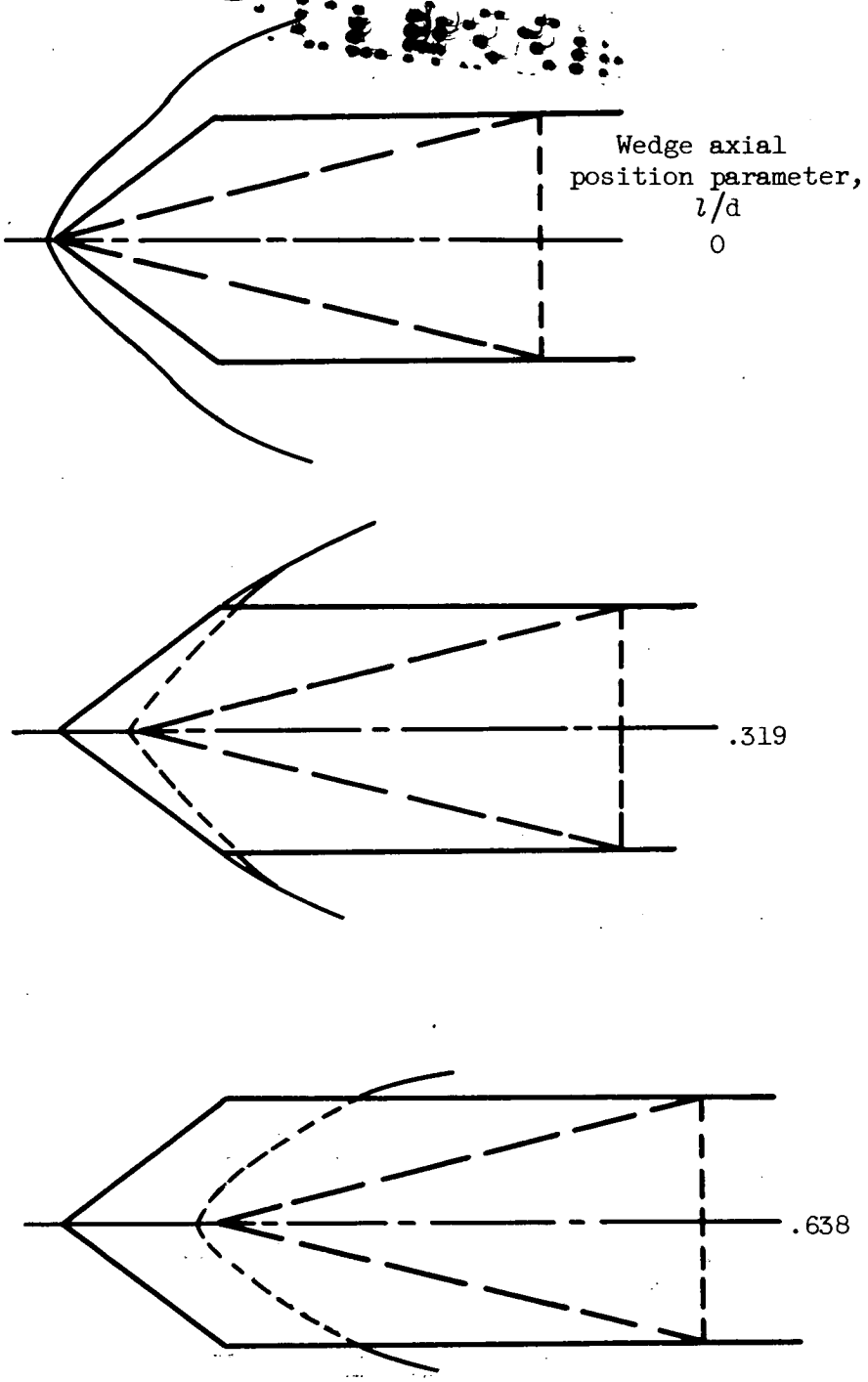


(a) Variation with wedge axial position parameter. Wedge included angle, 28°; h/δ, 0.856.

Figure 12. - Shock disturbance fields produced with several wedge configurations. Free-stream Mach number, 3.83.

[redacted]

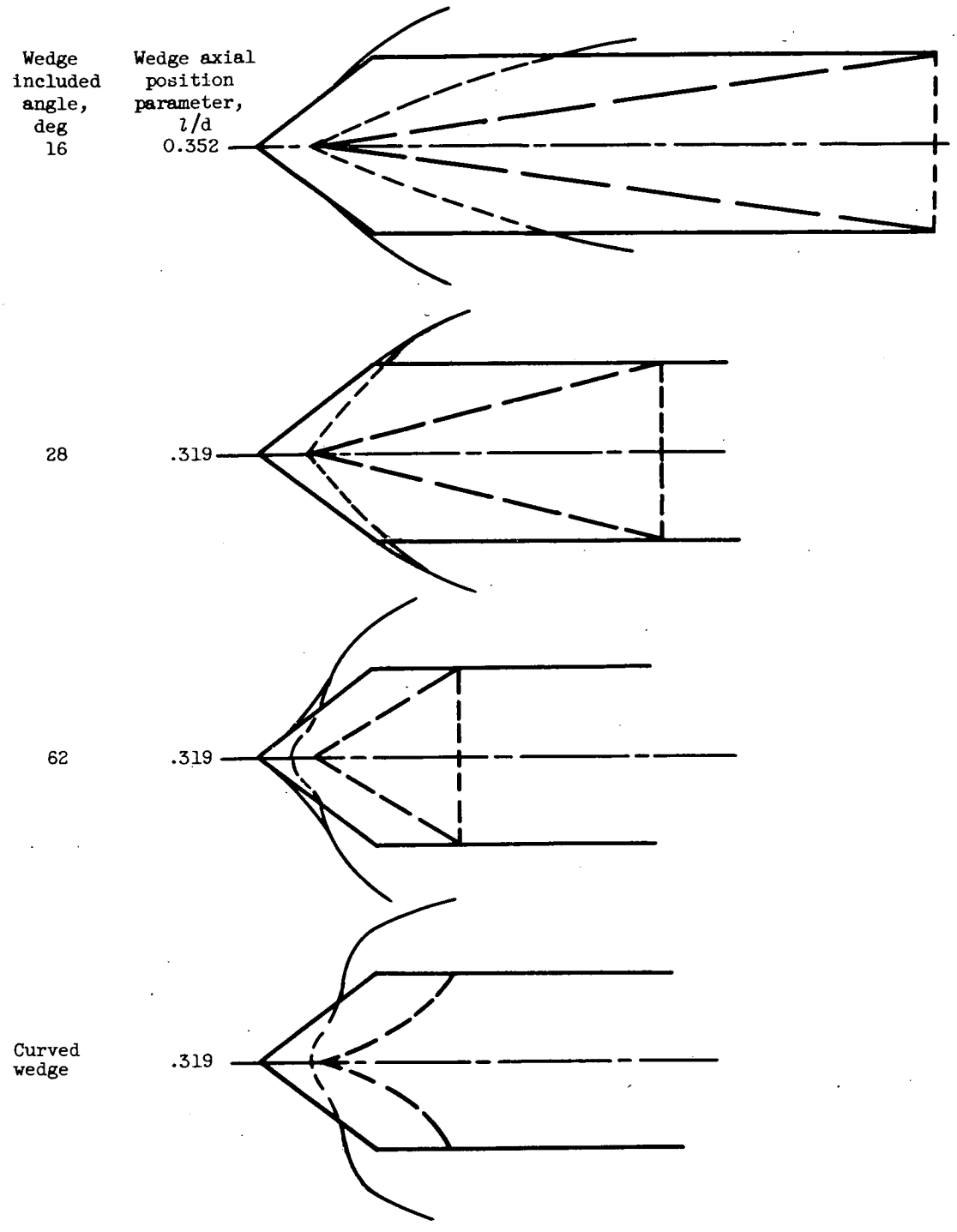


(b) Variation with wedge included angle. $l/d > 0$; $h/\delta$, 0.856.

Figure 12. - Continued. Shock disturbance fields produced with several wedge configurations. Free-stream Mach number, 3.83.

[redacted]

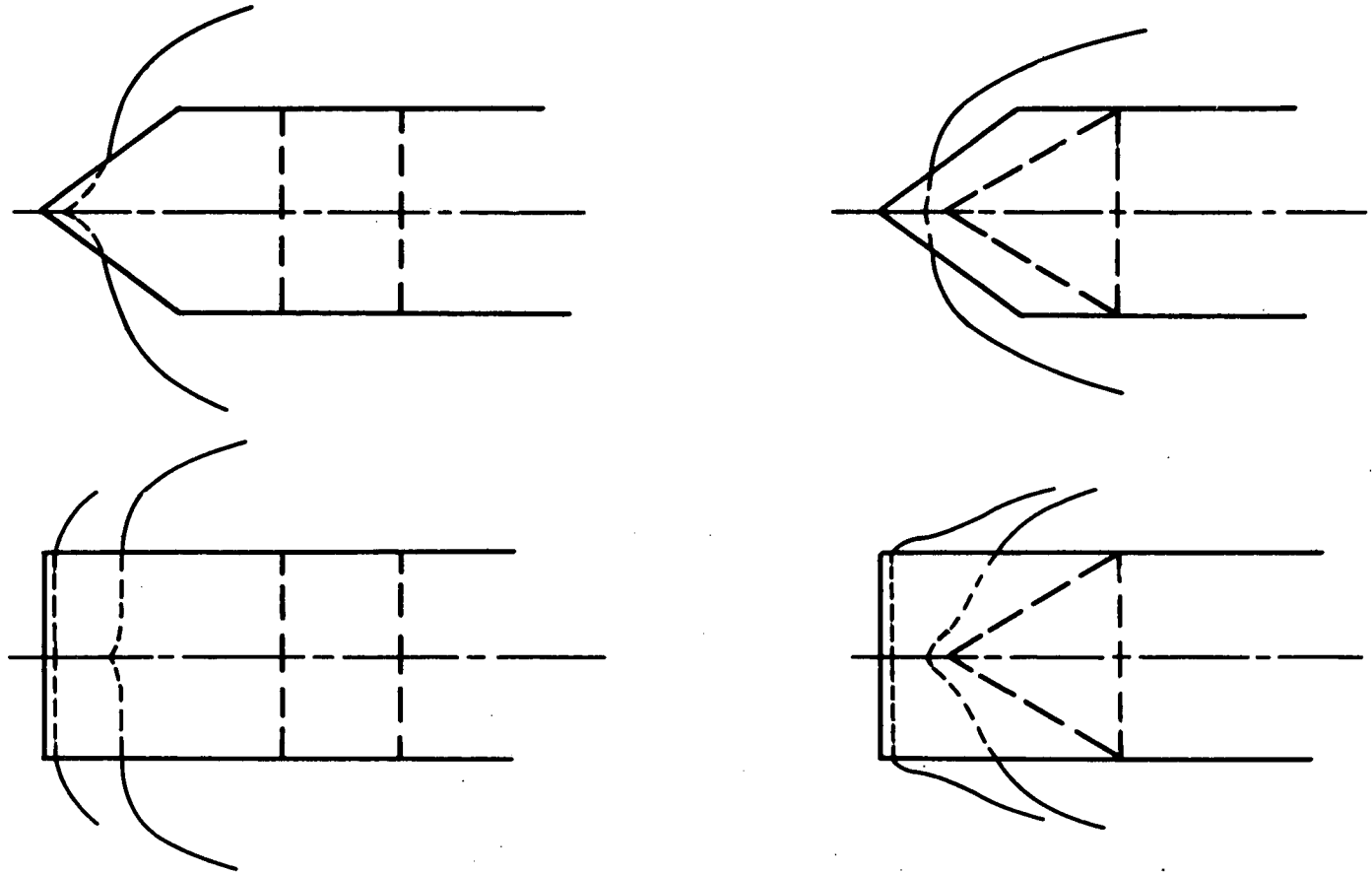

| | | |
|---|---|---|
| Wedge included angle, deg, | 180 | 62 |
| Wedge axial position parameter, $l/d$, | 1.148 | .319 |

(c) Variation with splitter plate. $h/\delta$, 1.284.

Figure 12. - Concluded. Shock disturbance fields produced with several wedge configurations. Free-stream Mach number, 3.83.

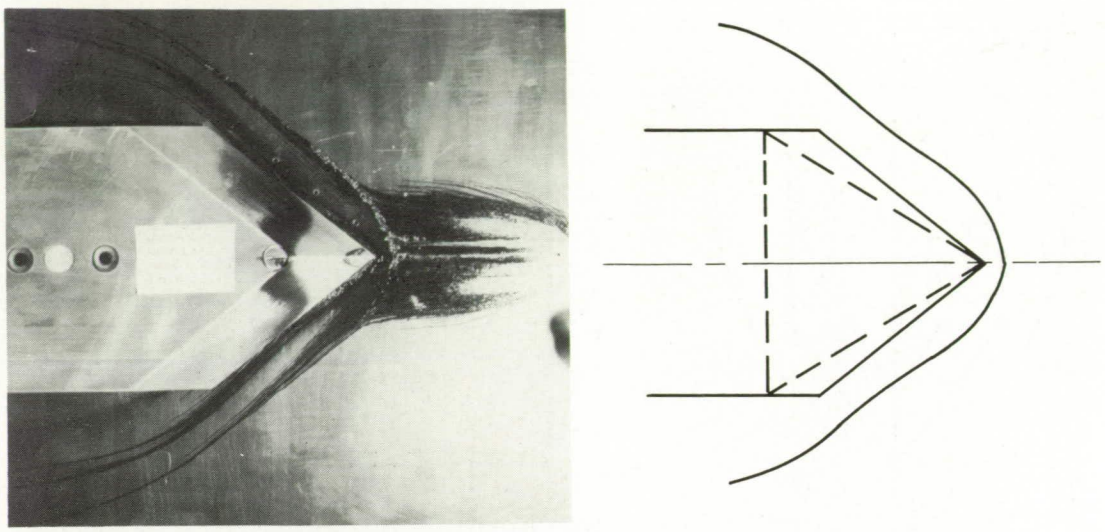

$l/d$, 0

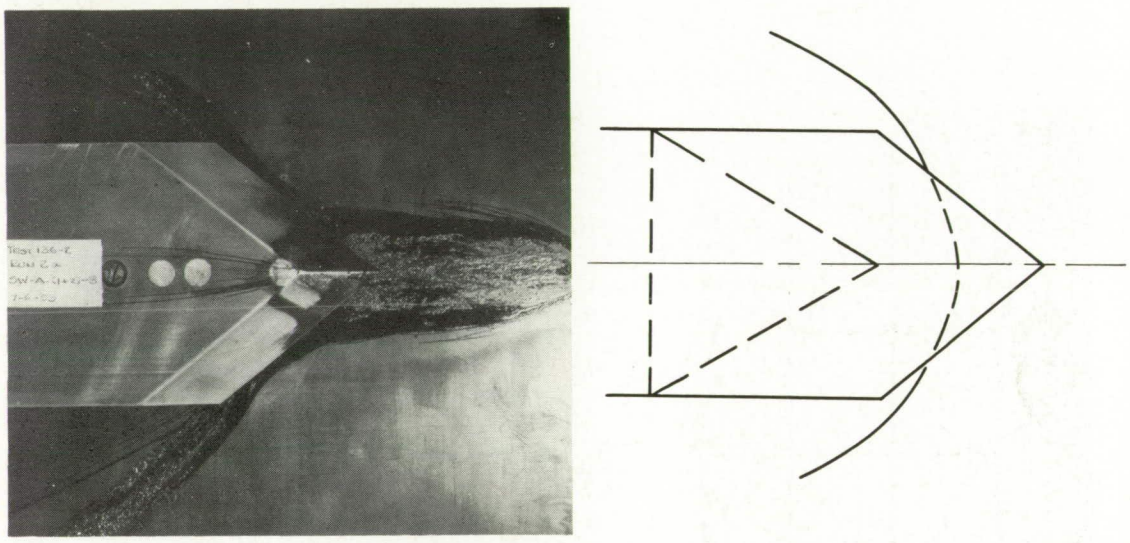

$l/d$, 0.638

C-34519

(a) 62° Wedge.

Figure 13. - Flow patterns for several wedge configurations at free-stream Mach number of 3.16 and wedge height parameter of 0.805.

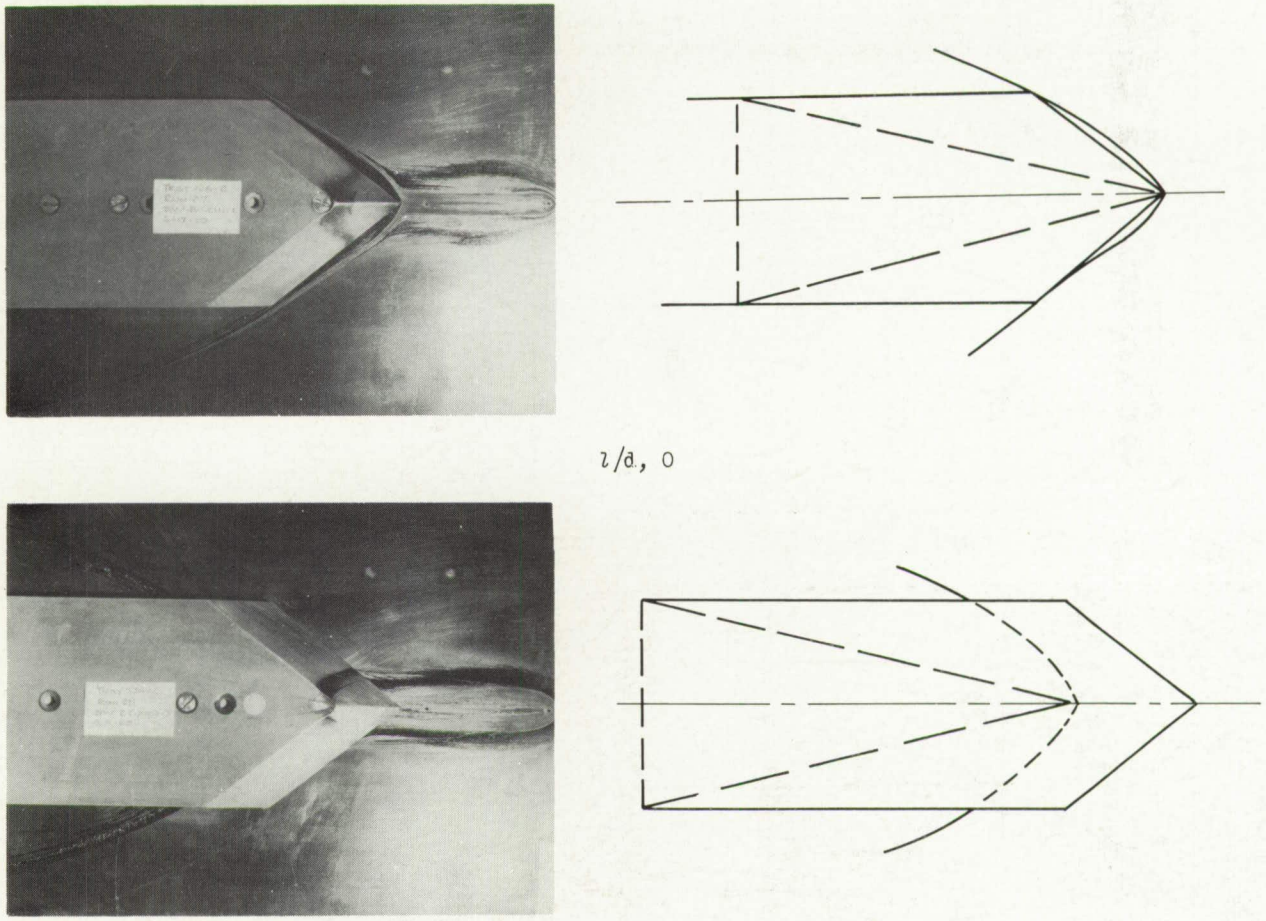


(b) 28° Wedge.

Figure 13. - Continued. Flow patterns for several wedge configurations at free-stream Mach number of 3.16 and wedge height parameter of 0.805.

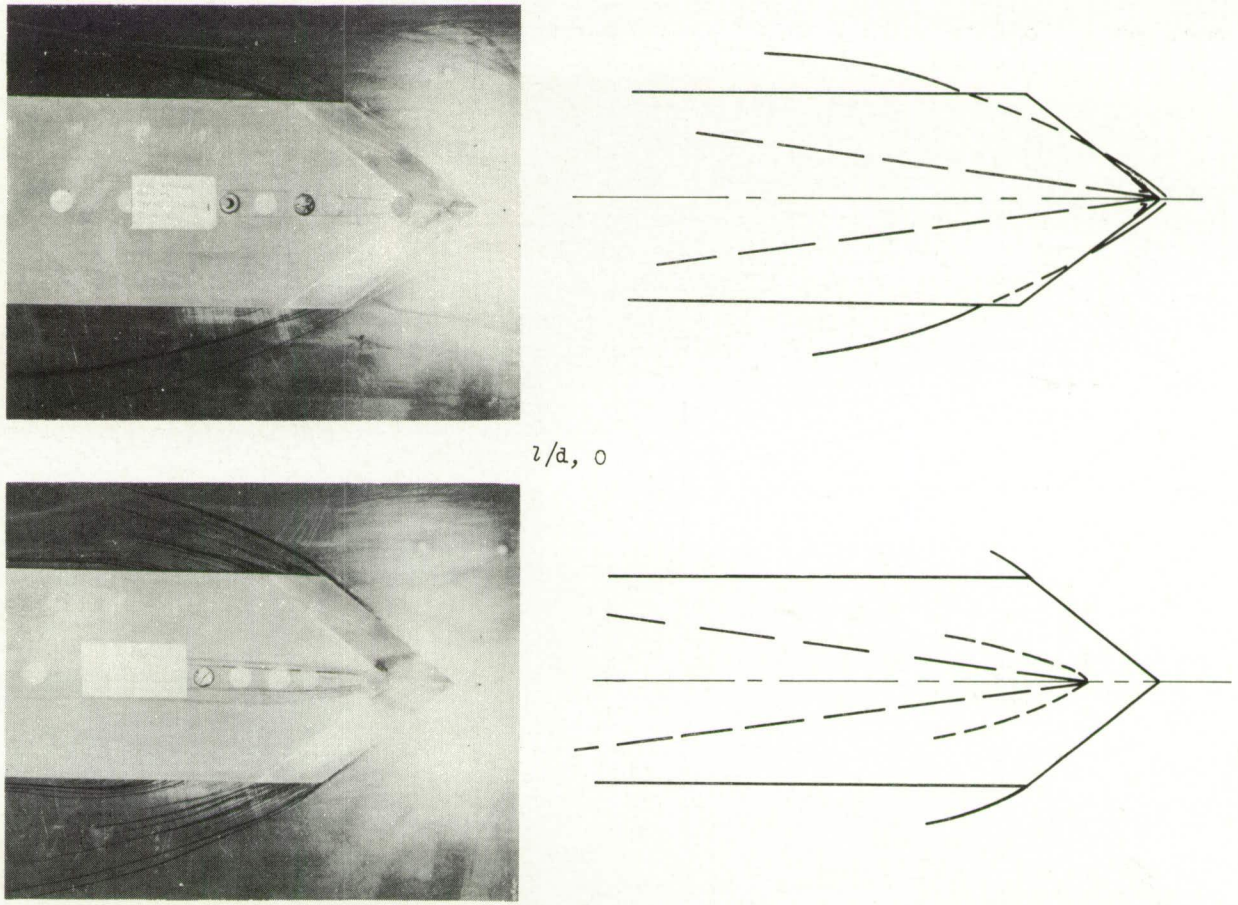


(c) 16° Wedge.

Figure 13. - Concluded. Flow patterns for several wedge configurations at free-stream Mach number of 3.16 and wedge height parameter of 0.805.

[redacted]